GLUCOSE CONCENTRATION AFFECTS FIBRIN CLOT STRUCTURE: MORPHOLOGICAL CHARACTERISTICS AND GLYCATION QUANTIFICATION

by

JACOB E. HOOD

(Under the Direction of Rodney D. Averett)

ABSTRACT

Hyperglycemia's influences on unstable and irregular clot formation in diabetes mellitus (DM) remains unclear because many factors known to influence fibrinogen to fibrin conversion, clot morphology, and thrombus formation present simultaneously in these patients. An LSM 880 (Laser Scanning Microscope) was used to analyze the effects of glucose concentration on fibrin clot structure; fibrinogen glycation was conducted to support characteristic findings. Algorithm outputs supported *in vivo* work and found that hyperglycemia, via increased fibrinogen glycation, alters fibrin clot structure at a fixed fibrinogen concentration. Additionally, 10 wt% S-Nitroso-N-acetyl-D-penicillamine (SNAP) was investigated to determine the efficacy in utilizing nitric oxide (NO) mechanisms to limit clot formation in hyperglycemic environments. Four 10 wt% SNAP polymer exposure conditions resulted in no polymerization and was likely a result of increased protein adhesion to the polymer film. NO was believed to further increase protein adhesion to the polymer as incubation with 10 wt% SNAP reduced dyed fibrinogen concentration significantly more (72.36%) than the non-NO releasing control.

INDEX WORDS: Fibrinogen, Hyperglycemia, Glycation, Feature Detection, Nitric Oxide

GLUCOSE CONCENTRATION AFFECTS FIBRIN CLOT STRUCTURE: MORPHOLOGICAL CHARACTERISTICS AND GLYCATION QUANTIFICATION

by

JACOB E. HOOD

B.S., The University of Georgia, 2016

A Thesis Submitted to the Graduate Faculty of The University of Georgia in Partial Fulfillment of the Requirements for the Degree

MASTER OF SCIENCE

ATHENS, GEORGIA

2018

GLUCOSE CONCENTRATION AFFECTS FIBRIN CLOT STRUCTURE:

MORPHOLOGICAL CHARACTERISTICS AND GLYCATION QUANTIFICATION

by

JACOB E. HOOD

Major Professor:	Rodney D. Averett
Committee:	Eric Freeman
	Hitesh Handa

Electronic Version Approved:

Suzanne Barbour
Dean of the Graduate School
The University of Georgia
May 2018

DEDICATION

I would like to dedicate the following work to my grandfather, William Edward Hood III, or *Jiddhu*, the Arabic name for grandfather – it's the name all 11 of his grandchildren called him. I was his oldest grandson and he taught me so much about family and treating others with respect. *Jiddhu* battled pancreatic cancer for three years and died two years ago, but I know he would have been proud of this accomplishment. He was a wonderful man and I am glad I was given the opportunity to dedicate this work to him.

ACKNOWLEDGEMENTS

I would like to thank the many people at the University of Georgia who assisted, guided, and contributed to my thesis. These individuals supported my research and without them I would not have completed the MS Biological Engineering program. First, I would like to give regards to my advisor, Dr. Rodney Averett, who was a continual source of advice and encouragement from the beginning of this study. Additionally, I would like to thank my committee members, Dr. Eric Freeman and Dr. Hitesh Handa, for providing thought-provoking questions and encouraging me to investigate and develop additional content areas of my thesis. I would also like to thank Marcus Goudie, PhD, and Dani Workman for their constant advice and unwavering willingness to supply materials. The nitric oxide portion of this experimentation would not have been accomplished if not for their approachability and expertise with biocompatible polymers. Lastly, I would like to thank my family for their continued love and support during this often stressful and frustrating time. I would not have been able to forge forward and complete my graduate studies without their reassurance and confidence in me. I love my family dearly.

TABLE OF CONTENTS

Page

LIST OF TABLES

Page

LIST OF FIGURES

Page

LIST OF EQUATIONS

Page

CHAPTER 1: INTRODUCTION

1.1 Purpose of the Study

The purpose of this study is to develop polymerization, fluorescence imaging, and computational techniques, and to examine the effects of glucose concentration on fibrin clot characteristics. The imaging technique of Laser Scanning Microscopy (LSM) is applied to quantify glucose concentration effects on fibrin clot morphology, and an Alexa Fluor® 488 (Fisher Scientific, Pittsburg, PA), a fluorescein derivative, is integrated into experimental protocols to successfully visualize variations in fibrin clot characteristics. Alexa Fluor® 488 contained purified fibrinogen with ~15 dye molecules per fibrinogen molecule and is said to be less pH-dependent and more photostable than fluorescein. Fibrinogen glycation is also quantified to support a hyperglycemic thrombogenicity theory; fibrinogen glycation is believed to influence fibrin clot formation and alter fibrin clot characteristics through a hyper-thrombotic shift in Virchow's Triad. The fibrin clot parameters of fibrin fiber overlap, fiber length, fibrin matrix porosity, and fractal dimension are selected to examine differences in these clot characteristics at a consistent and controlled fibrinogen concentration; fibrinogen concentration is consistently higher under hyperglycemic conditions and may conceal underlying effects of hyperglycemia on previous clot characteristics and glycation measurements. As such, the isolated effects of glucose concentration on clot formation are examined by measuring clot characteristics and fibrinogen glycation using this methodology. By comparing the results yielded for glycated and non-glycated clot characteristics, our understanding of hyperglycemic clot morphology is improved and the effects of glucose concentration on hyperglycemic thrombogenicity are explored.

Separately, 10 wt% S-Nitroso-N-acetyl-D-penicillamine (SNAP), is integrated into the initial glucose study to preliminarily assess the potential of using nitric oxide (NO) to influence clot formation in hyperglycemic environments. If successful, NO applications could be developed to limit hyperglycemic thrombogenicity and reduce associated clotting risks in hypercoagulable states. NO data is assessed to confirm NO release from developed polymer films by comparing NO release to a non-NO releasing control, N-aceytl-penicillamine (NAP); NAP is also examined to quantify NO-specific influences on glucose clot conditions through comparison to SNAP conditions. Fluorescence data are collected to confirm the presence of dyed fibrinogen in NO-exposed LSM conditions during polymerization. Experimentation with NO exposure is conducted to reveal NO's influences on fibrin clot characteristics, if any, and to analyze the potential of utilizing NO actions to reduce hyperglycemic thrombogenicity.

1.2 Expected Results

The goal of this thesis is to test the hypotheses that glucose concentration increases fibrinogen glycation and influences fibrin clot characteristics at a controlled and consistent fibrinogen concentration. With blood clot formation, secondary hemostatic response, fibrin generation, matrix development, and the characteristics of resultant fibrin matrixes, the primary focus in these experiments is to develop and apply image analysis algorithms to determine the effects of glucose concentration on the fibrin clot structure characteristics of fibrin fiber overlap, fibrin fiber length, fiber matrix porosity, and fractal dimension. Characteristics are expected to be comparable to other fibrin clot structure studies and unveil hyperglycemic effects on clot morphology. Specifically, the simulated non-treated diabetic condition (10.0mM glucose condition) is expected to present characteristics significantly different from other glucose (0.0mM and 6.0mM glucose) conditions and support hyperglycemia's influences on the

hemostatic response. Results are also expected to reflect the altered clot characteristics observed *in vivo* and justify hyperglycemia's added risk on hypercoagulability.

Fibrinogen glycation is expected to increase with glucose concentration and support hyperglycemia's influences on fibrin clot characteristics. Glycation is expected to be the highest in the 10.0mM glucose condition and decrease with decreasing glucose concentrations, but not necessarily follow a linear trend. This prediction is hypothesize because: 1) glucose is present in healthy physiology; 2) fibrinogen glycation occurs naturally at a native physiological glucose concentration; and 3) fibrinogen glycation at a native physiological glucose concentration is not believed to alter fibrin clot formation. Therefore, only significantly higher fibrinogen glycation levels would explain how increased fibrinogen glycation influences fibrin clot characteristics.

NO experimentation is expected to influence fibrin clot characteristics and be viable as a potential mechanism to limit thrombogenicity in hyperglycemic states. Specifically, integration of SNAP into incubation protocols is expected to limit clot polymerization and result in increased porosity measurements. Fibrin clots incubated with SNAP are expected to be measurably higher in fibrin matrix porosity when compared to non-NO-releasing counterparts. Furthermore, prolonged SNAP exposure is expected to further reduce clot formation and result in no fibrin formation with measurable NO release. Additionally, non-NO releasing control characteristics are expected to reveal insignificant variations when compared to original glucose condition characteristics. Given these hypotheses, 10 wt% SNAP integration is expected to support SNAP's potential to reduce thrombogenicity and limit hypercoagulability in hyperglycemic states by utilizing biological NO actions.

1.3 Novelty and Potential Outcomes

Many studies have examined fibrin clot characteristics, fiber properties, rate kinetics, and thrombus behavior in hyperglycemic conditions. However, this study is the first, to our knowledge, to examine glucose-specific influences on fibrin clot morphological characteristics in a controlled and consistent fibrinogen concentration system. Fibrinogen concentration is known to influence clot properties and has been variable in previous examinations where: 1) comparisons of physiological mimicked native and hyperglycemic fibrin clot characteristics were made *in vitro;* and 2) *in vitro* analyses of native and hyperglycemic blood (*in vivo*) were made. This is also the first study to quantify fibrinogen glycation in a controlled and consistent fibrinogen concentration system. Since variations in fibrinogen concentrations may influence fibrin clot characteristic and glycation results, this study's design is intended to corroborate previous fibrin clot characteristic and fibrinogen glycation work, and present novel data on hyperglycemia's influences on fibrin clot characteristics via an increased fibrinogen glycation mechanism. If glucose concentration has an effect on fibrin clot characteristics, the presented methodology may be applicable for clinical diagnosis. However, the protocols would have to be tailored to human plasma and coupled with the appropriate epidemiological data for medical use.

CHAPTER 2: LITERATURE REVIEW

2.1 Hemostatic Response and Fibrin Matrix Formation

Clotting components accumulate at the site of damaged endothelial lining to plug and repair tissue in response to vascular injury. For healthy individuals, balancing flow and sedimentation are continuously maintained through an intricate process known as hemostatic response [1]. Hemostatic response is an involuntary physiological mechanism that involves chains of chemical reactions, cell affinities, and coenzyme ion activations, and serves primarily to plug the damaged tissue, maintain blood flow conditions, and prevent the loss of blood with proper regulation [2-4].

Fibrin: The Thrombus Backbone. A blood clot, also known as a thrombus, is a biological matrix of erythrocytes, platelets, leukocytes, cholesterol and other macromolecules embedded within the formed connective network of crossed-linked fibrin fibers [3]. While the migration of activated platelets to the site of vascular injury initiates clot formation in a typical healthy response, it is the generation and development of a fibrin fiber matrix that maintains the structural integrity of a formed thrombus [1, 2]. As the fundamental component for clot development, maintenance, and lysis, investigation into fibrin generation, via its precursor molecule fibrinogen, has helped explore fibrinogen-fibrin, fibrin matrix formation, and morphological/behavior relationships in hemostasis [3, 5]. Studies have revealed fibrinogen relationships to fibrin generation and fibrin matrix formation under various systematic conditions, but associations between fibrin clot structure and fibrin clot strength for these conditions still require more controlled investigation to confirm isolated effects; several studies

have examined the effects of glucose concentration on fibrin(ogen) polymerization, lysis rate, and overall clot morphology, but none of these studies have quantified the isolated effects of hyperglycemia on these parameters or quantified fibrinogen glycation with controlled experimentation [6-8].

Fibrinogen History. Around the fourth century B.C., Hippocratic doctors first noted the presence of fibers in circulating blood plasma, but it was not until the seventeenth century that a distinct description of fibrinogen was transcribed [9]. While some debate exists regarding who should be accredited with the discovery of fibrinogen, (e.g., Rudolf Virchow claimed to have noticed the protein prior to P.S. Denis' 1859 work), P.S. Denis first coined the term *fibrinogen* as he attempted to purify the protein [9]. Specifically, Denis noticed the presence of fibrinogen, a soluble entity different from insoluble fibrin, while describing "a substance which [was] not at all fibrous" in the conclusion section of his "Mémoire Sur Le Sang" [9]. Although fibrinogen's structure, behavior in fluid, and roles in human physiology have been examined, a complete functional description in pathophysiology remains elusive [10, 11].

Fibrinogen Structure. Fibrinogen, a 340 kiloDalton (kDa) 46 nanometers glycoprotein, is comprised of two, three-paired polypeptide regions (Figure 1); two D-regions are linked to a central E-region domain through 29 disulfide bonds [12]. Each "half set" of D-region polypeptides, Aα, Bβ and γ-chains, are spherical in shape and contains both C and N-terminal ends. C-terminal ends extend on each side of the D-domain and meet on each side of the central E-domain at the N-terminal ends [13]. Further denaturing and isolation of fibrinogen has revealed polypeptide fragment weights of 63.5, 56, 47, and 7.05-kDa for the A, β, and γ chains and central E-domain, respectively [5, 12, 14, 15].

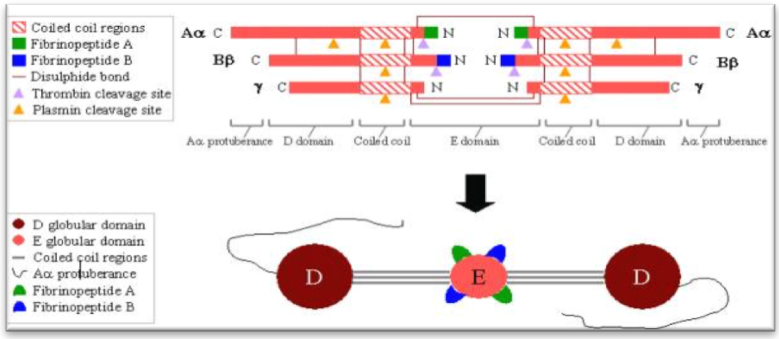

Figure 1: Structural composition of fibrinogen [16].

Fibrinogen-Fibrin Conversion. There has been a shift in characterizing fibrinogen's structure from a molecular model to one focused on fibrin generation via fibrinogen polymerization [17-22]. Specifically, fibrinogen converts into fibrin through thrombin-catalyzed removal of fibrinopeptides A and B from the N-terminal ends of the Aα and Bβ polypeptide [15]. Removal of fibrinopeptides A and B occurs via dissolution of four separate disulfide bonds on Arg-Gly residues of the E-region; dissolution exposes a terminal disulfide knot (NDSK) to generate a single fibrin monomer [12, 23]. During this conversion of fibrinogen into fibrin, monomers accumulate, interact intermolecularly, and attach to exposed NDSK via chemical signaling [17]. Oriented in 23-nanometer half-staggered fashion, repetitive binding of the D and exposed E-region, fibrin monomer binding grows into protofibrils (Figure 2) that are 600-800 nanometers in length; two fibrin monomer D regions may bind to a single exposed NDSK [24]. After protofibril formation, fibrin fibers, approximately ~100 nm in diameter, form by lateral and longitudinal interactions of fibrin αc-regions of protofibrils, but the conversion from protofibril to fibrin fiber is arguably the least understood mechanism of the coagulation cascade [24, 25]. Ultimately, conversion from fibrinogen to fibrin to protofibril to fibrin fiber forms the three-dimensional structure of an integrated fibrin matrix through lateral and longitudinal aggregation of fibrin fibers [18, 26, 27].

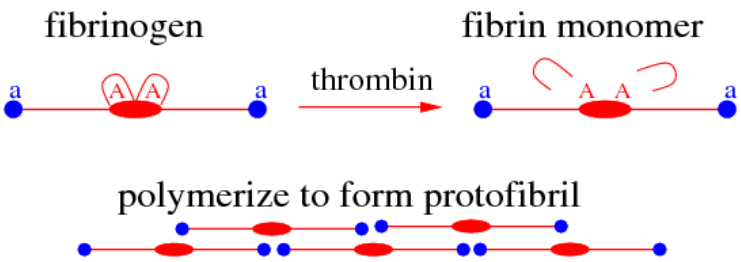

Figure 2: Fibrinogen cleaving and protofibril formation [28].

Fibrin Gels. The conversion of fibrinogen solution into a solidified fibrin matrix gel is distinguishable *in vitro* and has been characterized as when > 15% of the total fibrin accumulates and forms into an interconnected structure [29]. While the point of gelation is used clinically to establish clotting time, for example, through optical density, fibrin clot characteristics, the associated structural stability, and risk of clotting complications for a formed fibrin matrix are undistinguishable to the naked eye [27]. Physiological systematic conditions, like in the presence of disease or in macromolecule concentrations, are known to affect fibrin clot structure, but further experimentation is needed to better understand the pathophysiology of clotting, explain how systematic conditions influences clotting response, and comprehend how systematic conditions influence macrovascular disease development and hypercoagulability in particular at-risk conditions.

2.2 Fibrin Gel Imaging via Laser Scanning Microscopy

Scanning confocal microscopy (SCM) examines sub-cellular biological structures and functions by utilizing a distinctive combination of light and material properties. SCM utilizes isolated light planes to develop point-by-point cross-sections of a biological sample with improved rejection of out-of-focus noise and greater resolution than conventional imaging techniques [30, 31]. Unique to the SCM set-up, cross-sectional adjustment allows for both horizontal and vertical cross-sectioning of sample area without reducing image quality of interior

sections [30, 32]. Additionally, a curved confocal lens and pinhole aperture design generates a precise focal plane, eliminates light overload distortion, and increases image resolution to illuminate and reveal molecular structures, surface interactions, and bio-chemical dynamics at the nanoscale [30].

Scanning Confocal Microscopy. SCM often deploys a laser of adjustable light intensity in a technique known as Laser Scanning Confocal Microscopy (LSCM) to help distinguish interior sections of a biological sample; LSCM is becoming increasingly popular in cellular biology, molecular biology, neurobiology, biochemistry, and other physical sciences due to the simultaneous development of highly specific biological fluorophores and improved light analysis capabilities [33]. Through the physical phenomenon known as Stokes Shift, LSCM uses the physical property of fluorescence to release light photons at a longer wavelength than originally absorbed by a source laser. Fluorescence is exhibited (Figure 3) when the material is excited into a state of "high vibrational energy" by the incoming light photons from the source laser [32]. Fluorophores, biochemical molecules that exhibit the physical property of fluorescence, covalently attach to amino acid residues, proteins, antibodies, or cellular organelles have been developed to accurately visualize molecular-scale components with improved spatial resolution dynamically [31].

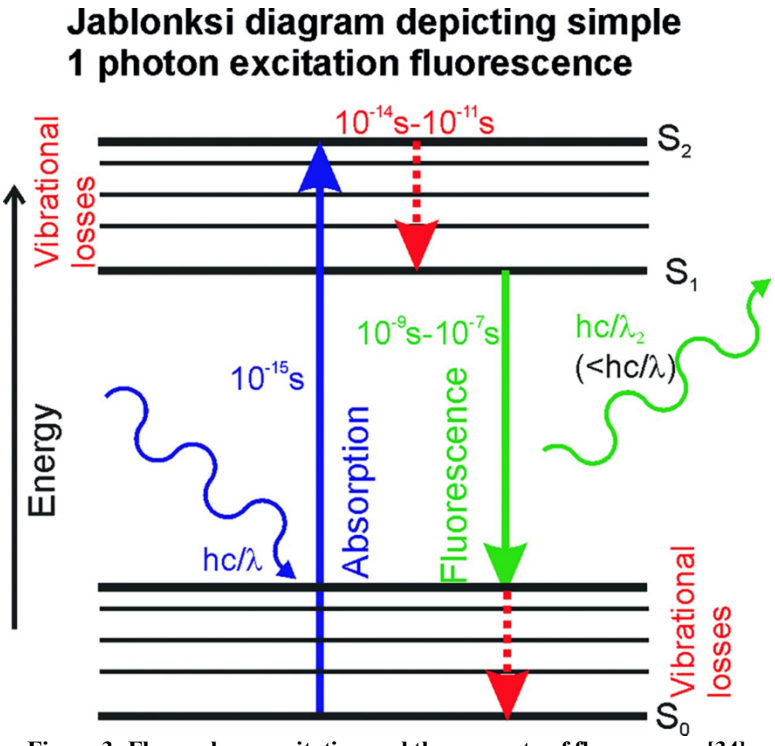

Figure 3: Fluorophore excitation and the property of fluorescence [34]

Fluorescent Tagging. Parallel to the development of new imaging techniques, photon releasing molecule development has simultaneously helped experimentation. Numerous fluorophore derivative protein labels are now available for direct covalent attachment to C-H and N-H bonds on nucleic acids, and these photon-releasing molecules are continuously modified to meet intensity, photostability, and wavelength specifications for optimal compatibility with biological samples [32]. Fluorophores are characterized based on the maximum absorption/emittance of the material, and fluorophore physical properties are exploited for LSCM application. Based on origin and molecule size, fluorescent molecules are categorized into the three major groups: organics dyes, green fluorescent protein (GFP), and quantum dots [35]. Countless subclasses of these groups have been generated to meet the desired fluorescent properties mentioned above, but in general, these three main classes present with some consistent characteristics [36]:

1. Organic dyes, for example, fluorescein, have improved photostability and solubility;

2. GFPs, cloned from the jellyfish *Aequorea Victoria,* generate significantly higher light intensity; and
3. Quantum dots have excitation and emission wavelengths distinct from other fluorophores.

While each of these classes has distinct advantages and disadvantages, instability and toxicity with GFPs and quantum dots makes organics dyes the most commonly used fluorophores for physiologically relevant biological sampling [37].

Epifluorescence Microscope Design. Once a fluorophore is selected for LSCM application, the necessary laser to exploit the unique absorption and emission characteristics of the sample's fluorophores must be isolated [31]. For epifluorescence microscope configuration (Figure 4), the light source and detection aperture align the same optical path, so it is easiest to explain LSCM methodology by following the single light path [38]. First, the light source from the laser passes through emission filters to seclude undesired wavelength(s). Upon isolation, the filtered excitation laser passes through a dichroic mirror with confocal design to concentrate the beam path and remove out-of-focus light for cross-section scanning [39]. Concentrated light then passes through an objective aperture to further control the light beam; dimensions of cross-sectional area scanning are regulated by physical manipulation of the objective aperture size [38]. Once the beam path reaches the cross-sectional sample area, fluorophore, non-fluorescent, and non-excited source light photons emit from the sample, pass back through the objective aperture, and reach the dichroic mirror [38]. The dichroic mirror material, not the confocal design, reflects photons shorter than the known fluorophore wavelength which include photons below the emission of the fluorophore, and isolates fluorophore photons from the total emission

beam [40]. Finally, fluorophore photons reach the detector aperture for image generation, but image processing is required to quantify incoming photon data.

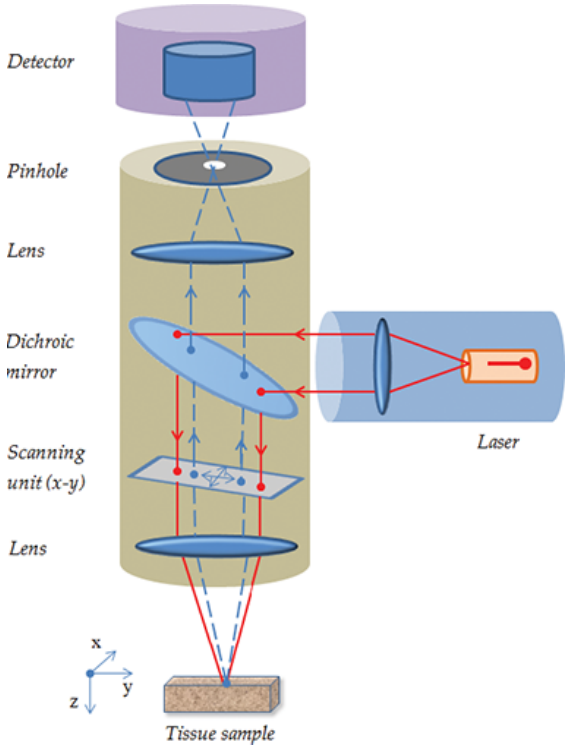

Figure 4: Laser Scanning Confocal Microscopy (LSCM) components in an epifluorescent configuration

Image Processing. Once light reaches the detector aperture, emittance, intensity, and duration of incoming photons must be analyzed. Photomultiplier tubes are integrated into LSCM technique to help distinguish small variations in light intensity; photon properties are translated into a current to increase data precision, but the data are still a result of light diffraction [41]. Therefore, light diffraction adjustment is necessary to account for light dissipation because the photomultiplier tubes only convert a fraction of total sample emission and unfocused photons hinder the fraction of converted data [38, 42, 43]. While epifluorescence is designed to control the amount of light that travels to the detector aperture, the point-spread function (PSF) accounts for fluorophore excitation probability of relating the distribution of the light, light intensity, numerical aperture, possible range of refraction angles, and refractive index of the medium under

a point source assumption; a central disk surrounded by concentric rings is produced for every detected fluorophore under this point source assumption by relating the radius of the central disk to the non-dimensional number numerical aperture [41, 44]. Overall, this is a simplistic description of epifluorescence, but, generally, LSCM utilizes fluorophore emittance to develop a resolved digital image of a biological sample by utilizing light properties and the PSF summations for all excited fluorophores in a sample [38].

Fibrin Gel LSCM. Biological imaging, image quantification, and fluorophore capabilities have undergone major advances, and LSCM applications have been applied to fibrin gel imaging. While characterization of fibrin clot structure is limited for native conditions (Figure 5) and far less defined for variable systematic concentrations and diseased states, LSCM has characterized fibrin clot structure in current literature [7, 8, 45]. Specifically, fibrin clot structure characterization examined fibrin diameter, fibrin density, fiber branching, fiber length, pore size, and thrombus growth and has also validated that fibrin clot structure is dependent on the conditions in which clotting components are suspended [18, 20, 27, 46-49]. However, further fibrin clot experimentation, fibrin gel imaging, and image quantification are needed to improve the uncertainty remaining with fibrin clot structure characterization [20, 50]. Specifically, the effects of glucose concentration on fibrin clot characteristics can be quantified through controlled experimentation to differentiate how hyperglycemia may be influencing thrombogenicity in at-risk hypercoagulable states by applying a LSCM technique.

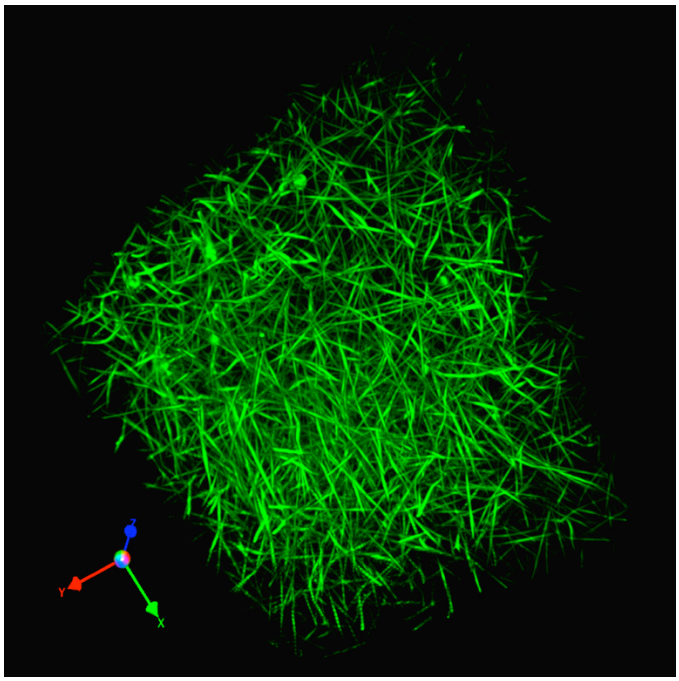

Figure 5: A three-dimensional reconstruction of a native fibrin gel with Alexa 488 dye using fluorescent scanning confocal microscopy [51]

2.3 Diabetes Mellitus: A Prothrombotic State

The current understanding of hypercoagulability, thrombosis, and coagulation afflictions on human physiology can be accredited to the initial work of German pathologist, Rudolf Ludwig Karl Virchow (1821 - 1902), who was the first to relate cellular pathology to disease origin [52]. Known today as Virchow's Triad, Virchow hypothesized that three factors (Figure 6) promote hypercoagulability, and hypercoagulable states are defined using three interconnected factors: 1) stasis or changes in blood flow; 2) inflammatory responses or changes that affect the endothelial wall; and 3) intrinsic blood alterations or changes in the blood's functionality [53]. While a broad understanding of how these factors influence hypercoagulability exists, the basis for thrombosis initiation remains fundamentally unknown because of understanding of healthy hemostatic response remains rudimentary; this has made it difficult to define acute irregularities of hemostatic response and explain irregular response etiologies. Additionally, many factors

systematic conditions have shown to simultaneously influence thrombosis, which has made it difficult to distinguish direct/indirect effects on Virchow's Triad *in vivo* [54-58]. Additionally, while hypercoagulable states are defined by a statistical risk of thrombosis from clinical imbalance of blood movement, vascular damage, and/or irregular protein quantity or functionality, a state of hypercoagulability does not ensure thrombosis manifestation and not all occurrences of thrombosis have similar etiologies [59]. Despite the lack of explicit causes for thrombosis initiation, the establishment of hypercoagulable states have helped to prevent vascular events, limit thrombogenesis, and reduce thrombotic incidence in at-risk individuals [55, 56, 60, 61].

One factor that meets the criteria of a hypercoagulable state is the diseased state of diabetes mellitus (DM), as this chronic condition is notorious for vascular complications [62, 63]. However, DM also consistently presents with other factors known to promote thrombosis (e.g.,, hyperinsulinemia, dyslipidemia, hypertension, obesity, decreased fibrinolysis, endothelial dysfunction, and platelet aggregability) and the true effects of the disease on thrombosis risk remain muddled [54, 64, 65]. While a full understanding of the disease's influences on thrombogenicity remains elusive, resting hyperglycemia, the defining characteristic of DM, is believed to promote thrombotic risk because the increased risk of and macrovascular events for these individuals cannot be completely explained by the typical cardiovascular risk factors seen in these patients. Additionally, glycemic control, in such situations as HbA1c reduction > than 0.5%, has shown to significantly decrease thrombogenicity in some cases to suggest high circulating glucose concentrations encourage irregular and spontaneous clots to develop [54, 62-65]. There have been many proposed hypotheses to explain a hyperglycemic thrombogenicity, but more hematological research is necessary to: 1) improve prediction of thrombosis in

hyperglycemic states; 2) define the true effects of established factors on hemostatic response; and 3) expose the underlying mechanisms by which these defined factors influence thrombosis initiation. Controlled experimentation examining hyperglycemia's true influences on clot formation may be helpful due to the multitude of variables known to influence hemostatic response *in vivo*. Additionally, exposing the isolated effects of glucose concentration on hemostatic response could help shed light on hyperglycemic thrombogenicity influences and help reduce clotting risk in cases where glycemic control fails.

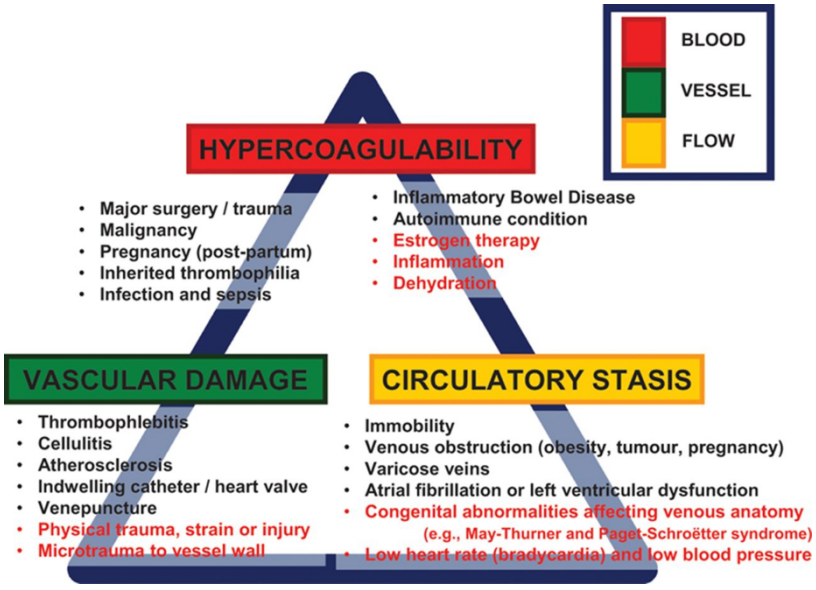

Figure 6: Virchow's Triad and its influences on cardiovascular health [66]

History and Categorization of DM. DM is, by definition, a metabolic condition of compromised carbohydrate, lipid, and protein metabolism [67]. Specifically, the blood protein insulin is deficient and there is inadequate insulin secretion and/or diminished cell response to insulin; this results in resting hyperglycemia, which is used for DM diagnosis [68, 69]. The first description of DM dates back approximately 3000 years, yet arguably, the clinical diagnosis and treatment of DM has been slow to develop. Diabetic symptoms were first described by ancient Egyptians depicting insects attracted to the frequent urination of emaciated individuals.

However, it was Matthew Dobson, a chemist working in an evaporation lab, who qualitatively distinguished the presence of sugar in diabetic urine in the mid-17th century [70, 71]. Over a century later, Karl Trommer developed the first chemical tests to measure the concentration of glucose in blood/urine in the 19th century, and this basic concept is still used to diagnose and monitor diabetic patients [70-72]. DM is categorized into two main types: Type I Diabetes (DM1), or insulin deficient diabetes, defined by an immune deficiency, and Type II Diabetes (DM2), or non-insulin dependent diabetes, defined by hyperglycemia [73]. This study focused on explaining hyperglycemia in DM2 because DM2 accounts for 90-95% of the total DM condition and is diagnosed by resting hyperglycemia [74]. Today, although patients self-monitor glucose levels and self-administer diabetic treatment, DM is only therapeutically treatable; it remains one of the largest medical inflictions and is associated with serious acute and chronic health risks [71].

Diabetes Epidemiology: A Concerning Prevalence. The prevalence of DM worldwide can no longer be considered just a medical inconvenience. Currently, more than 30 million individuals in the United States, approximately 10 percent of Americans, have DM and worldwide totals are projected to rise to 522 million by 2030 [71, 75]. From a historical viewpoint, with the development of 19th century chemical testing able to accurately identify and measure hyperglycemia, DM2 diagnoses have steadily increased (Figure 7), but it is the recent increase in DM2 (4.7% to 8.5%) since the 1980s that concerns epidemiologists [76-78].

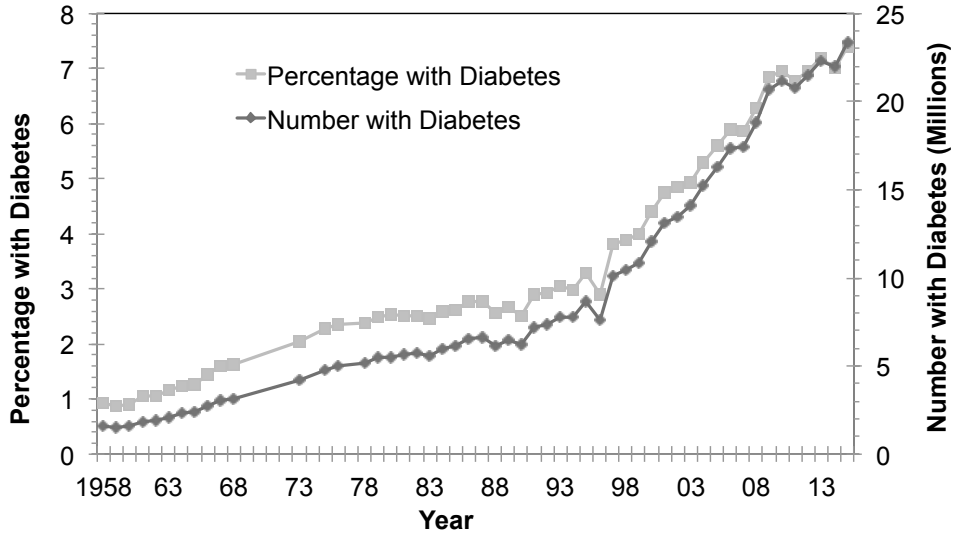

Figure 7: Diabetes Mellitus diagnoses trends in the United States over the last ~70 years [75]

First, the rate of DM2 in adults (Figure 7) is projected to continually increase over the next two decades. Additionally, clinicians, researchers, and health advocates project that more than 90% of total DM diagnoses will be DM2 diagnoses; due to a less active and more obese society throughout the world, a majority of this percentage increase will occur in developing countries where treatments are less accessible [71, 75, 79]. Second, there is a concern for the increase rate of undiagnosed and untreated DM2. In 2011, over half of DM2 individuals (183 million) remained undiagnosed with a large percentage residing in developing countries [71, 75, 79]. This is concerning because individuals with undiagnosed and/or untreated DM have a lower life expectancy and are at higher risk of serious clotting complications compared to DM2 individuals undergoing treatment [71, 75, 79]. While current financial estimations only account for medical costs of treated diabetic patients, average medical costs for DM2 individuals are 2-5 times higher [80-83]. The future economic burden of DM requires immediate responsiveness because both the prevalence of DM2 and rate of undiagnosed/untreated DM2 are projected to reach high proportions that have catastrophic consequences. Currently, the annual health care (Figure 8)

contribution of DM in the United States is estimated at 322 billion (20% of medical care costs) and these medical costs can be directly correlated to two major components: blood glucose maintenance and thrombotic vascular events [80-83]. Glycemic control has shown to lower thrombotic risk in some cases, but an improved understanding of the hyperglycemic thrombogenicity relationship could further lower lifetime DM2 medical spending, alleviate some of the economic healthcare burden, and limit thrombogenesis in DM2 patients where glycemic control has not been successful [82, 83].

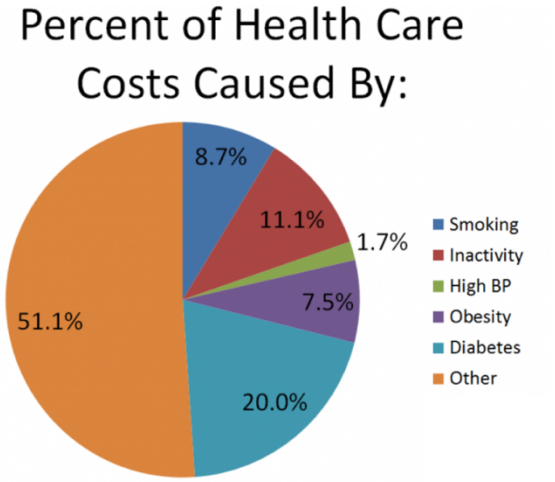

Figure 8: Percent contribution medical costs of DM in the United States [84]

Diabetes and Cardiovascular Conditions. Thrombosis has a profound effect on DM2 as more than 80% of diabetic-related deaths are due to thrombophilia, and DM individuals are four times more likely to develop a cardiovascular condition [64, 81, 85, 86]. Cardiovascular disease (CVD) is a term that accounts for all irregular clotting and vascular conditions [85]. As the leading cause of death in the United States, cardiovascular events have shown to be 37.2% higher for individuals with DM2; CVD conditions contribute significantly to DM medical costs and mortality as DM is an independent risk factor for arterial CVD, cerebrovascular disease, peripheral vascular disease, acute myocardial infarction, stroke, peripheral artery disease, venous

thromboembolism and atherosclerosis [64, 85, 87-89]. While CVD accounts for over 30% of the world's mortality, accounting for all types of CVD afflictions are too cumbersome to address [64, 85, 87-89]. The CVD sub-entity condition, venous thromboembolism (VTE) has been widely addressed because of DM's association with spontaneous thrombus formation; spontaneous thrombus formation is associated with a tangible shift in Virchow's Triad and could be explained by hyperglycemia's influence on fibrinogen glycation [64, 90-94].

Typically characterized by conditional/locational afflictions of the lower extremity, VTE is separated into two distinct stages: deep vein thrombosis [95], or spontaneous thrombus formation, and pulmonary embolism (PE), or dissociation and translocation of the formed thrombus [95, 96]. Statistically, VTE affects as many as 2 million people each year in the United States, but it is the 30% of PE occurrences that result in sudden death that are of the most concern [97]. While controversy over hyperglycemia's direct risk for VTE incidence still exists, data from DM studies suggests that hyperglycemia has a pronounced effect on thrombogenicity and spontaneous thrombus formation [91, 93, 97, 98]. In a 2005 age-adjusted study, a two-fold higher incidence of VTE was reported for DM2 patients. Similarly, VTE risk was found to be 60% higher after controlling for weight in a 2001 meta-analysis of DM2 patients with previous VTE history [91, 99]. Several epidemiological studies validate increased DVT and PE incidence in DM2 individuals [64, 97, 100, 101]. Supportively, the occurrence of DVT increases inflammatory response which further promotes thrombosis suggesting that DM patients with previous DVT history may be at particular risk for VTE and other complications when glycemic control has failed [102]. With the current economic burden estimated at $5.5 billion for DVT and $15 billion for PE, DM contributes significantly to total VTE medical costs. As the effects of glycemic control on VTE occurrence have yet to be confirmed, through analysis of fibrin clot

characteristics, further experimentation could provide an improve understanding of hyperglycemic influences on a platelet poor system, consistent with DVT.

A Hyperglycemia Prothrombotic Shift. Three main independent mechanisms (Figure 9) are consistently presented in the literature to explain hyperglycemic thrombosis initiation and DM thrombogenicity: indirect oxidative stress, endothelial dysfunction, and altered coagulation protein activity via direct glycation [64, 103]. While oxidative stress and endothelial dysfunction mechanisms are linked to platelet activation, platelet involvement in venous thrombosis is unclear. Some studies suggest that the role of platelets in venous thrombosis has limited significance due to immobilization, but recent examinations suggest that platelets may play a more significant role in venous thrombosis than previously believed [103, 104]. Although all three hypotheses likely have profound influences on venous thrombosis *in vitro*, altered coagulation protein activity via direct glycation was the focus of the current VTE study because of its believed influences independent of platelet's role in clotting response. Venous thrombosis is qualitatively a platelet-poor system, and altered coagulation protein activity alone via direct glycation, may be able to justify a pro-thrombotic shift in Virchow's Triad. More conclusively, however, altered coagulation protein activity contains the most consistent supporting evidence for hyperglycemic thrombogenicity in DM.

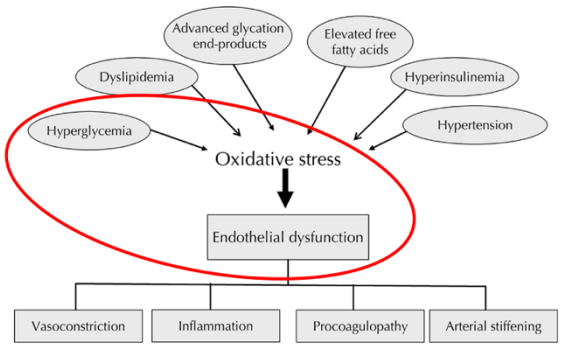

Figure 9: Hyperglycemia and other influences on thrombotic risk [64]

The coagulation cascade is a highly integrated and sensitive process with changes in coagulation protein activity or concentration having serious influences on thrombogenesis via measured changes to fibrin clot properties, fibrin clot structure, and clot behavior. With independent links to irregular clotting, late stage vascular events like in micro/macro-vascular disease, fibrinogen concentration is consistently higher in all hyper-thrombotic states. Fibrinogen has been reported to be particularly higher for DM patients, for instance, DM patients with no history of vascular complications measure a 50% increase in fibrinogen concentration when compared to the 2.5 mg/mL seen on average in healthy individuals [105-108].

The concentration of fibrinogen has a profound effect on thrombotic risk due to its correlation with hemoglobin A1c, the established hyperglycemia measurement, suggesting that hyperglycemia further influences thrombogenesis in DM2. Hemoglobin A1c has been previously linked to thrombogenicity and vascular risk to imply both hyperfibrinogenemia and hyperglycemia influence pathogenesis of venous thrombosis through alterations in coagulation protein activity of fibrinogen via direct glycation [105, 106, 109]. Resulting from the covalent binding of reducing sugars and protein, glycation is a natural process of metabolism that occurs at physiological temperatures. Contrary to enzymatic glycosylation, which is highly regulated and integral to cellular function, non-enzymatic glycation is a spontaneous process of metabolism that may actually alter protein functionality. Therefore, the combination of hyperfibrinogenemia and hyperglycemia found in DM2 may further promote venous thrombosis due to the increased rate of fibrinogen glycation found in DM2 individuals. Direct correlation between DM2 and glycated fibrinogen was found to be approximately twice (7.84 vs. 3.89 mol glucose/mol fibrinogen) that of non-diabetic patients in a 38-individual comparative study [110-113].

Furthermore, glycation of fibrinogen has shown to alter fibrin clot properties and overall clot behavior. Although the exact mechanism behind altered fibrin gel properties in patients with diabetes is unclear, a shift in hemostasis via direct glycation justifies how changes in fibrin clot structure promotes atherosclerosis and stimulates thrombogenesis. Specifically, glycated fibrinogen has shown to develop more compact clots that are less porous, more rigid, more branched, less permeable, and comprised of thinner diameter fibers [46, 114-117]. In a Pieters et al. 2008 study, the hypothesized hyperglycemic mechanisms that alter protein functionality were examined in DM2 individuals through glycemic control (insulin treatment) to investigate fibrin network characteristics with decreased fibrinogen glycation. After glycemic control, there was significant decreases in fibrinogen glycation (6.81 to 5.02 mol/glucose/mol fibrinogen) and the rate of lateral aggregation (5.86 to 4.62), and significant increases in permeability (2.45 to 2.85 x 10^{-8} cm^2) and lysis rate (3.08 to 3.27 μm/min) suggesting hyperglycemic influences on fibrin network formation kinetics; fiber thickness also increased after glycemic control and there was no difference in glycemic control and non-diabetic fiber diameter suggesting that hyperglycemia may play a large role in fiber thickness that impacts permeability and lysis rate [101]. Additional examination of the physiological behavior of glycated fibrin clots suggests that these clot characteristics make diabetic individuals more resistant to fibrinolysis and molecular studies have shown glycation occurs at lysine and valine residues, βK133 and γK75, close to plasmin cleaving sites [118-121]; while not the focus of this presented study, molecular examination of fibrinogen's glycated resides may provide further justification to a hyperglycemic caused thrombogenicity theory.

While hyperglycemia influences thrombotic risk in DM2, not all evidence supports altered coagulation protein activity via the direct glycation hypothesis. In a 2016 study, Li et al.

examined the mechanical properties of individual fibrin fiber formed from diabetic blood plasma to evaluate the effects of fibrinogen glycation on a single fibrin fiber. Using atomic force microscopy and fluorescent microscopy, fibrinogen glycation was found to have "no significant systematic effect on single-fiber modulus", but significantly decreased with increasing fiber diameter, or the density of the protofibrils connection. Since fiber modulus is a material constant and is not dependent on the diameter of homogeneous material, it was hypothesized that fibrin fibers do not have homogeneous cross-section of uniformly connected protofibrils which may be influenced by increased glycation. While the lateral assembly of protofibrils is poorly understood and stands as a major pitfall in the current clot literature, Li et al. (2016) suggested that fiber diameter including fibrinogen, glucose, or thrombin concentrations strongly affects fiber modulus. Since thin fibers have shown to be more than 100 times stiffer than thick fibers, glycated fibrin fibers must have decreased lateral protofibrils density connections and develop fibrin clots with thinner periphery fibers. While Li et al., (2016) found glycation did not have a direct effect on single-fiber mechanics, it was still found to affect overall fibrin clot structure and fibrinolysis.

The pathophysiology for venous thrombosis remains elusive, and so, answering how hyperglycemic mechanisms influence thrombogenesis is complex and multifaceted. While DM2 is often associated with poor health outcomes, hypotheses for hyperglycemic thrombogenicity are often inconclusive, contradictory and likely influence all stages of coagulation. Therefore, while fibrin clot structure may influence thrombus formation, clot susceptibility to lysis, and thrombogenesis, it is likely a combination of hyperglycemia, (either directly or via protein glycation), oxidative stress, endothelial dysfunction, and other factors that impact CVD risk. However, further examination into hyperglycemia's influences on fibrin clot structure

characteristics may further explain how hyperglycemia and increased glycation influence thrombogenesis with the proposed experimentation.

2.4 Potential Thrombotic and Glycemic Nitric Oxide Control

Nitric oxide (NO) is a free radical gas that plays complex regulation roles in human physiology (e.g., angiogenesis, inflammation and infection, vasodilation, thrombosis, smooth muscle cell proliferation and migration, wound healing, and cellular metabolism) [122-128]. However, NO is only a local mediator, likely only inducing physiological response ~100 μm from its origin, due to its reactivity with hemoglobin in blood circulation [129]. Although NO's reactivity initially suggests a limited role in cardiovascular health, a cell-free layer adjacent to the vascular lining provides natural diffusive resistance to NO consumption to support NO's dynamic influences on maintaining healthy vasculature, and regulating hemostatic response [130]. Additionally, endothelial dysfunction and deficient NO concentration have been linked to arterial stiffness, hypertension, atherosclerosis, and cardiovascular diseases to further support the profound impact NO deficiency has on thrombotic pathogenesis [131, 132]. Despite all evidence in support of NO's role in vascular health, some researchers still argue NO has limited potential as a therapeutic agent because continuous and steady NO generation is necessary to influence physiological responses and the current methods to overcome NO's reactivity and supply continuous NO flux, although continue to improve, remain limited [133, 134]. Yet, others argue NO's reactivity provides a unique opportunity for biological regulation and control due to easy clearance from blood circulation [133, 134].

With steady and continuous NO release, NO-containing species, called NO-donors, have been extensively examined to overcome the challenges associated with NO's reactivity, deliver NO release continuously, and provide NO-mediated functions for therapeutic clinical

applications [135]. Many NO-donors have been investigated, each with specific clinical characteristics including those with specific NO release rates or material strengths, but S-nitrosothiols (RSNOs) present a superior potential therapeutic application for hyperglycemic thrombogenicity because of their limited influence on vascular tolerance, biocompatibility in medical polymers, significant antimicrobial and antithrombotic effects, and prolonged NO release for clinical use [136]. In particular, SNAP presents with these characteristics as literature supports its ability to limit thrombosis, increase vasodilation, and influence coagulation messaging through NO release.

Additionally, while NO flux has shown to play an important role in glucose metabolism and some NO mechanisms have been hypothesized to regulate blood glucose in diabetic patients, these results are not absolutely congruent in SNAP experimentation. Ultimately, SNAP potential to simultaneously limit thrombosis, reduce platelet activation, and lower plasma glucose concentration in hyperglycemic conditions provides a promising potential platform for efficacy in limiting thrombogenicity in hyperglycemic states. Additionally, as the complexity of study advances steady NO-release, via an NO-donor, NO-release would be necessary to counteract the NO scavenger hemoglobin and analyze NO influences with flow dynamics and cellular components such as red blood cells (RBC) and platelets.

Characterizing S-nitroso-N-acetylpenicillamine. Evidenced from supporting literature, SNAP provides a great potential vessel to release NO and control physiological responses for biomedical applications. With a general RSNO structure, a nitroso group attached to the sulfur atom decomposes under photolytic, heat, and/or catalytic conditions via homolytic cleavage of the S-N bond (Figure 10); decomposition of RSNO results in the release of NO and generation of a disulfide [137].

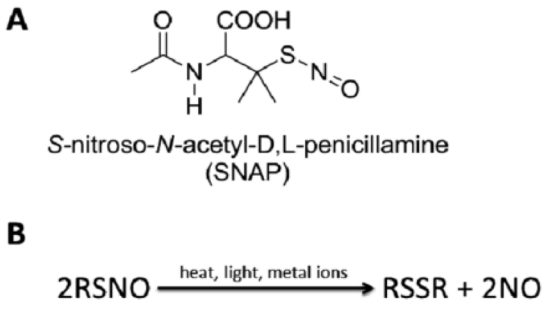

Figure 10: (A) The chemical structure of S-nitroso-N-acetylpenicillamine (SNAP) and (B) S-nitrosothiol decomposition [138]

While no RSNO has reached the stage of clinical application, the discovery of natural thiol-containing proteins, e.g., cysteine, glutathione, and albumin, further supports the biocompatibility of NO-donors to successfully overcome NO's reactivity for biomedical applications [139]. These naturally occurring NO-donors provide further evidence of potential NO control mechanisms and much experimentation has been conducted to improve the rate, duration, and stability for both endogenous and exogenous donors in recent years [138, 140]. Furthermore, synthetic RSNO, SNAP, provides a unique opportunity to examine NO-specific actions because of its biocompatibility. The nitrosating biocompatible parent molecule to SNAP, N-acetyl-D-penicillamine (NAP), is a FDA-approved drug used to treat heavy metal poisoning, and so, NAP is used as a control (Figure 11) when examining the NO-specific actions of SNAP because it decomposes similarly, albeit without NO delivery [141, 142].

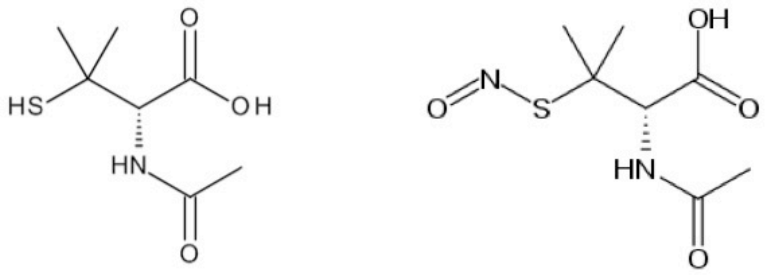

Figure 11: Chemical compositions of N-acetylpenicillamine (Left) and chemical compositions of S-Nitroso-N-acetyl-D-penicillamine (Right)

S-nitroso-acetylpenicillamine (SNAP) Vasodilation. Despite its simplistic chemical composition and convoluted mechanisms for generation, regulation, and metabolism, NO has known vasodilation and endothelial turnover functions [130]. Generated by one of three human nitric oxide synthase (NOS) enzyme isomers, endothelial NOS (eNOS), NO can be synthesized (Figure 12) through the conversion of L-arginine to L-citrulline [128]. At a physiological rate between $0.5 - 4 \times 10^{-10}$ mol min^{-1} cm^{-2}, NO migrates from inside endothelial cells to the interface between the vessel wall and lumen to maintain endothelial lining and regulate clotting response; specifically, NO activates guanylate cyclase in the presence of oxygen or nicotinamide adenine dinucleotide phosphate-oxidase (NADPH), and several other required cofactors to have a profound influence on smooth muscle relaxation [128, 131, 132, 143]. Vasodilation, the natural widening of a blood vessel via smooth muscle relaxation, creates localized flow conditions that disfavor thrombosis by increasing blood flow, decreasing vascular resistance, lowering blood pressure, and slowing the heart rate [144]. Conversely, guanylate cyclase inhibition promotes vasoconstriction which has shown to facilitate thrombogenicity via hypoperfusion or inadequate oxygen and nutrients exchange [145]. In light of this NO-vasodilation relationship, S-Nitrosothiols (RSNOs) have been studied to examine vasodilation capabilities. Supportively, studies have found that SNAP is a potent vasodilator via a continuous NO release mechanism;

bolus microinjections of SNAP caused dose-dependent vasodilatation (5.83 +/- 0.17) in endothelium-intact arteries that was supported by recovery to pre-injection pressure upon vascular clearance [146].

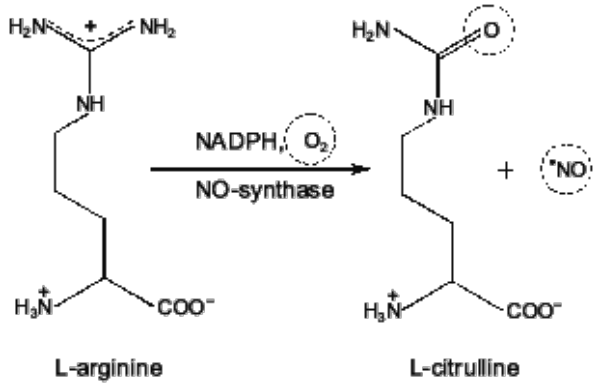

Figure 12: L-arginine to L-citrulline conversion via endothelial nitric oxide synthase [147]

S-nitroso-acetylpenicillamine (SNAP) and Fibrinogen Polymerization Inhibition. In addition to SNAP's pronounced vasodilation response, SNAP-doped Elast-eon E2As catheters have shown to simultaneously reduce thrombus area (1.56 cm^2 vs. 5.06 cm^2) when compared to control catheters; reduction in thrombus area in the presence of RSNOs may be explained by significant structural changes to fibrinogen that modify protein functionally and, therefore, alter polymerization [148]. In the presence of excess thrombin, bovine fibrinogen polymerization (2.5×10^{-5} s^{-1}) decreased by approximately 60% and 68% in the presence of 20μM and 50μM RSNOs, respectively, and profound inhibition was measured when polymerization was repeated with human fibrinogen [148]. Encouragingly, the same concentration of RSNO had no effects on tosyl glycyl prolyl arginine-4-nitroanilide acetate, a chromogenic substrate for thrombin, suggesting that fibrinogen inhibition was substrate specific. Further experimentation suggested conformational changes to fibrinogen caused polymerization inhibition because identical CD spectra of RSNO and native fibrinogen solutions were seen, no free thiols were measured in

solution, and, chemically, all fibrinogen thiols are involved in disulfide bridges [149]. However, SNAP has been found to limit fibrinogen polymerization by approximately 50%, with maximum inhibition of 64%, with RSNO-aromatic ring binding in the C-termini α-chains; this finding supports SNAP-induced polymerization inhibition with an ~11-15% change in α-helical content of fibrinogen [149].

Influences of Nitric Oxide on Platelet Activity and Fibrinogen Adhesion. While the main focus of this study is the examination of secondary hemostasis and fibrin clot formation, NO's influence on platelet activation is briefly addressed because primary hemostasis in the form of the generation of the platelet plug inherently effects secondary hemostasis and NOs most established physiological regulation role is platelet inactivation; platelets are not integrated into this experimentation, but evidence in support of NOs effect on limiting platelet activation provides a path for further experimentation. In the activated state, platelets, or leukocytes, are non-nucleus bound cells that promote thrombus formation (Figure 13) through three distinct phases: 1) adhesion or the attachment of platelets to the vessel wall; 2) further activation or the chemical signaling to recruit more platelets, fibrinogen, and other components necessary for clot polymerization; and 3) platelet aggregation or the binding of activated platelets to other activated platelets [150, 151].

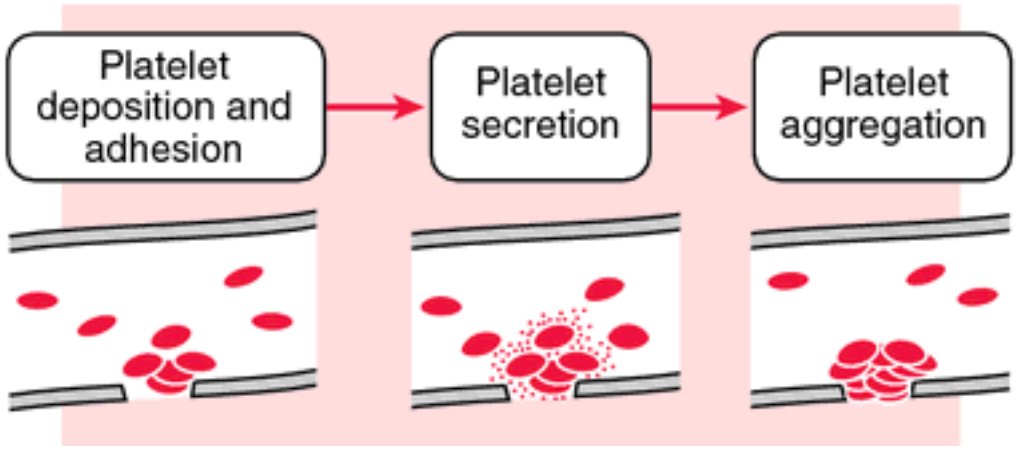

Figure 13: The three phases of platelet plug formation. (Left): adhesion, (Middle): further activation via chemical signaling, (Right): platelet aggregation.

Therefore, as NO regulates platelet activation and platelet aggregation, NO provides a protective response to platelet recruitment and platelet plug formation after primary hemostasis initiation [152]. In this regulation response, platelet NOS (pNOS) synthesizes NO, in a similar fashion to eNOS, to stop platelet activation and ensure that thrombi do not propagate or occlude the vessel diameter after initial thrombus growth [144, 153, 154]. Although a concrete understanding of NO's role in platelet activation is not fully defined, it is clear that NO concentration regulates platelet plug formation by decreasing platelet activation as a pNOS inhibitor, L-NAME, significantly increases platelet recruitment, platelet aggregation, and thrombus size via a cyclic GMP-dependent mechanism [155]. In contrast, platelets incubated with SNAP cause significant reduction ($p < 0.05$) in adhesion to fibrinogen-coated micro-titer plate surfaces at a physiologically relevant 0.0125 U/mL thrombin level [156]. Additionally, a flow-based material study of SNAP-E2A coatings showed to reduce platelet activation via increased NO concentration, as platelet count (100 ± 7% vs. 60 ± 6%) was preserved when compared to E2As control circuits [157]. While SNAP-E2A coatings also increased fibrinogen adsorption, whereby SNAP/E2A coatings fibrinogen concentration dropped 13% over the 4

hours measurement, the release of NO was able to overcome increased fibrinogen adsorption and limit thrombus formation by inactivating platelets. As fibrinogen adherence has been linked to thrombus formation via binding of activated platelet to the integrin receptor, αIIb-β3, on each end of the fibrinogen molecule during platelet plug formation, SNAP provides thromboresistance via platelet inactivation in addition to the fibrinogen polymerization inhibition and vasodilation effects [157-159].

NO's Mechanism for Glucose Metabolism. In addition to the NO-mediated vasodilation and platelet activities, NO's role in glucose metabolism is noted for regulating and improving clotting response in diabetes as cellular NO synthesis plays a critical role in glucose metabolism [160]. NOS expression modulates glucose transport to skeletal muscles and adipose tissues, and control of plasma glucose concentration could limit hyperglycemic direct glycation of fibrinogen and reduce the thrombogenicity experienced in these patients [160]. Specifically, these cell types are believed to remove glucose from the blood for cellular growth via two major stimuli, insulin and muscular contraction, and the glucose transporter, GLUT4, facilitates the removal of glucose from the blood in both pathways [133, 161]. While the insulin pathway innately requires insulin binding for glucose disposal, the muscular contraction pathway utilizes NO generation to mediate glucose uptake that is independent from the insulin concentration, and this is of particular importance for the control of plasma glucose concentration as insulin deficiency is a consistent characteristic of diabetic patients [160]. Supportively, inhibition of eNOS has shown to reduce leg glucose uptake by 48% in healthy individuals and a more pronouncedly ~75% in DM2 patients [162, 163]. As analysis found this inhibition to be independent of blood flow or insulin level, it was suggested that up-regulating NO production had the potential for plasma glucose control [162, 163]. In support of these claims, NO-donors have been examined for

glucose metabolism control, but results have been conflicting. While exposing NO-donor sodium nitroprusside (SNP) has shown to inhibit glycogen synthesis and increase the rate of glucose transport in rat skeletal muscle, SNAP presents a conflicting effect on glucose metabolism [164]. Concentrations of S-Nitrosoglutathione (GSNO) and SNAP below 1mM increased basal 2-deoxyglucose uptake, for example, at 115.8 +/- 10.4% with SNAP and 116.1 +/- 9.4% GSNO with a maximum at 1mM, and appeared to be additive with insulin exposure in the adipocytes of both control and diabetic rats, but these same donors demonstrated significant inhibition at a decrease of 50.0 +/- 4.5% and 61.5 +/- 7.2%, respectively at concentrations above 10mM [165].

Although micromolar concentrations of RSNOs support NO-mediated glucose uptake, the NO-donor is suggested as the cause for affecting glucose metabolism. RSNOs have shown to reduce plasma insulin levels and cause a hyperglycemic effect, but more recent experimentation has shown that NOs inhibitors, like L-NMMA and L-NAME, decrease the NO-donor hyperglycemic effect by up-regulating the NO-mediated glucose metabolism pathway and counteract the decreased glucose tolerance with SNAP administration [166, 167]. Overall, there is still much experimentation required to examine the effect of all of these NO-mediated mechanisms in physiology, but the presented literature offers a promising potential of NO-donors, particularly of SNAP, to reduce thrombogenicity in hyperglycemic conditions by simultaneously reducing thrombosis, regulating platelet activation, and lowering plasma glucose concentration.

CHAPTER 3: AIMS AND OBJECTIVES

3.1 Objectives

In this study, the biological imaging technique of laser scanning confocal microscopy (LSCM) is used to quantify differences in fibrin clot morphology at three different physiological blood glucose concentrations. Specifically, the fibrin clot structure features of fiber overlap, fiber length, fibrin matrix porosity, and fractal dimension are measured via image detection of fibrin matrix aggregates. Algorithms are employed to distinguish fibrin clot features through glucose concentration comparisons. An improved understanding of the effects of glucose concentrations on fibrin clot structure could be used to improve the prevention and treatment of thrombotic clotting states like that seen in DM. If significant mean differences are found between glucose conditions, the presented experimental design could be modified to provide an alternative quantitative tool for the predication of diabetic-related clotting risk; however, this methodology would need to be tailored to human blood and coupled with the appropriate epidemiological data for diagnostic purposes. Task-oriented objectives were designed to achieve the following project aims:

1. Present experimental protocols for the successful polymerization, imaging, and quantification of fibrin clot structure.
    - Can fluorescence, object detection, and computational techniques be used to visualize fibrin clot structure?
2. Develop image analysis algorithms to quantify fibrin fiber overlap, fibrin length, and matrix porosity for sample conditions.

- Does glucose concentration affect fibrin clot structure?

3. Conduct statistical analysis to determine if mean differences exist between conditions for the four outcomes of interest.
    - Do results suggest that this methodology could be adapted for human sampling and clinical diagnosis of clotting risk?
4. Integrate SNAP into **Objective 1** and revisit/address supplemental questions.
    - How does SNAP integration affect fibrin clot structure outputs?
5. Evaluate the efficacy of NO-release for thrombotic control.
    - Could SNAP integration reduce the hyperglycemic condition seen in DM patients that cause thrombotic risk?

Examination of the glucose/nitric oxide/fibrinogen interactions could also provide a proof of concept for reducing thrombogenicity in physiological hyperglycemic conditions. Overall, the effects of glucose and SNAP on fibrin clot structure are presented in hopes of providing explanations for mean differences in fiber overlap, fiber length, fibrin matrix porosity, and fractal dimension using a LSCM approach. If significant mean differences are found between glucose conditions, the current experimental design could provide a novel platform to limit hyperglycemic thrombogenicity though NO-medicated glycemic control, while simultaneously improving hemostatic response.

3.2 Experimental Approach

Both experimental and computational methodologies were integrated into this study to achieve the following main aims:

Experimental Methods. Native and glycated fibrin clot protocols were developed to mimic physiological thrombus formation; glucose concentrations of 6.0mM and 10.0mM were selected

to meet the approximate fasting blood glucose averages of healthy and untreated diabetic patients, respectively [168]. For all incubation protocols, a 48-hour incubation period was applied to facilitate non-enzymatic glycation of fibrinogen at a physiologically relevant temperature of 37°C. For fibrin gel preparation, elevated platforms were created to maintain the native structures of formulated clots and protect samples from dehydration and contamination. Clots were polymerized with a uniform concentration of 1 U/mL Human thrombin and repeated with an extreme concentration, 50 U/mL Human thrombin, for instance in which no clot formation was detected; this was conducted to confirm the lack of fibrin clot formation was not due to a lack of enzymatic activity. Uniform imaging area, zoom, polymerization time, and pixelated areas were selected for examination through a trial-and-error phase; all comparison were conducting under identical data collection parameters to further remove an uncertainty associated with the feature detection algorithms developed. Z-stacks vertical slicing of samples was conducted on representative areas of fibrin gels conditions and repeated at least three times per trial sample to ensure results represented the true characteristics of the condition; z-stack slicing was conducted at a consistent interval of 0.5 μm and uniform for all LSM conditions. A variety of biological assays were developed to supplement fibrin clot characteristics and support literature comparisons. Fibrinogen glycation was quantified using a colorimetric glucose assay and compared to previous literature when assessing its accuracy and validity.

Computational Methods. Pre-processing and image analysis were conducted separately for each 2-D slice of fibrin clot structure parameter calculations; fiber aggregates were highlighted using image analysis techniques in Matlab (MATLAB; The MathWorks, Natick, MA) for fiber detection and thrombus feature classification. Computational methods were developed to distinguish fibrin clot structure parameter differences in fibrin fiber overlap, fiber length, fiber

matrix porosity, and fractal dimension at the selected glucose concentration. Z-stacks were pre-processed to enhance fibrin matrix structure prior to image detection and analysis; fibrin clot characteristic calculations were measured separately for each 2-D slice of a z-stack. "Vesselness" and line generation were conducted using the fibermetric (Equation 1) and Hough Line transform functions [169].

Equation 1: Equation for the vesselness measure of a 2D image where B and C are thresholds that control the sensitivity of the line filter, RB is the dissimilarity measurement, and S is the "second-order structureness" of a given dimensional area.

$$\mathcal{V}_o(s) = \begin{cases} 0 & \text{if } \lambda_2 > 0, \\ \exp\left(-\frac{\mathcal{R}_B{}^2}{2\beta^2}\right)\left(1 - \exp\left(-\frac{\mathcal{S}^2}{2c^2}\right)\right) \end{cases}$$

The fiber metric function was applied to generate a binary pre-processed matrix, while the Hough Line transform functions were applied to obtain image analysis outputs of fiber overlap and fiber length [7, 169, 170]. Prior to Hough Line generation, fiber matrix porosity and fractal dimension were measured by dividing the number of "on" pixels by the total number of pixels for each pre-processed 2-D binary image. Line segments represented detected fibrin fibers, generated from the tubular structures of the fibermetric function and were utilized to conduct all subsequent calculations. Fibrin fiber overlap was determined by computing the number of overlaps (intersections) for each individual fibrin fiber (Appendix A). Simultaneously, fiber length outputs were determined by measuring the length of each generated Hough Line. Fiber length outputs were converted from length averages (in pixels) of the Hough Lines from each z-stack slice into a quantifiable measurement in microns (μm). Generation of tubular structures and line segmentation (Figure 14) followed this identical methodology for each raw tagged image file of a z-stack.

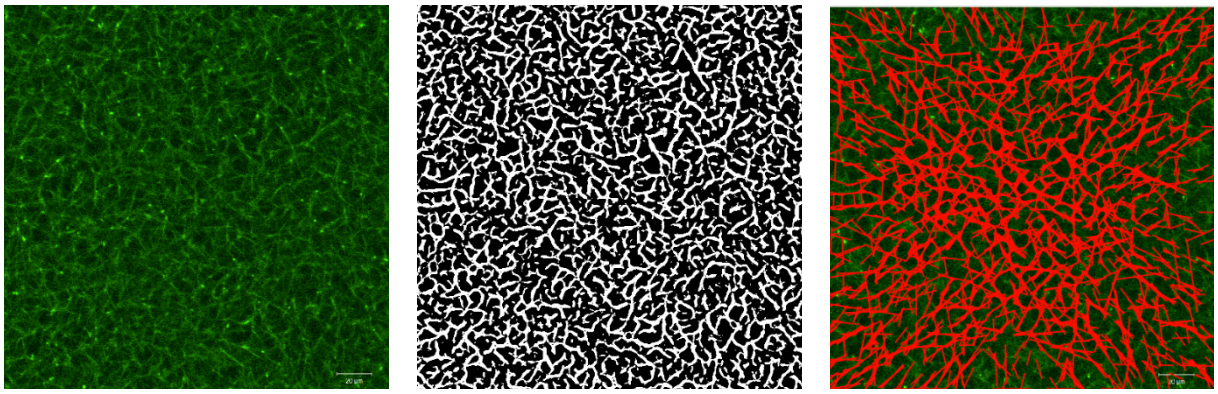

A B C

Figure 14: (A) 2-D z-stack slice TIFF file (B) Conversion of (A) to a binary pre-processed matrix using the fibermetric function (C) Line segmentation of the TIFF file using Hough line transform functions.

CHAPTER 4: GLUCOSE EXPERIMENTATION

4.1 Materials and Methods

The following two methods were used in this research: 1) feature detection of fibrin clot characteristics at three glucose concentrations; and 2) evaluation of fibrinogen glycation using a colorimetric glucose assay. Glucose conditions were conducted at a controlled and consistent fibrinogen concentration to assess the isolated effect of glucose concentration on feature detection measurements and fibrinogen glycation.

Material Preparation. Three glucose conditions, 0.0mM, 6.0mM, and 10.0mM, equal concentrations of FIB 3 Plasminogen, von Willebrand Factor and Fibronectin depleted (ERL, Southbend, IN), and fibrinogen from Human Plasma, Alexa Fluor 488 Conjugate (Fisher Scientific, Pittsburg, PA) were integrated into 100 μL volumes. The three incubation conditions contained 6.8 g/L fibrinogen, 100mM NaCl, and specified amounts of glucose; a 10% dye of fibrinogen was applied to working volumes to match previously successful imaging of fibrin gels [7, 8]. A stock 40mM glucose solution (TGDI) was prepared from D-glucose and deionized water, diluted with 50mM Tris buffer (Lonza, Basel, Switzerland), and stored at 4°C prior to use. For each glucose condition, 30 μL of stock TGDI was further diluted with 50mM Tris buffer to meet specified concentrations of glucose; a 20.0mM glucose solution was created for integration into incubation of the 6.0mM glucose condition and a 33.3mM glucose solution was created for integration into incubation of the 10.0mM glucose condition. For the 0.0mM glucose condition, 30 μL of 50mM Tris buffer was used in lieu of TGDI to maintain a consistent total incubation volume for a three incubation conditions. Two μL of 5M NaCl were added to each 100 μL

volume to meet a physiological sodium concentration during incubation [171]. Volumes of materials (Table 1) to meet the specified incubation conditions were mixed in 1.5 mL centrifuge tubes and incubated at 37°C in a 5L Isotemp Water Bath (Fisher Scientific, Pittsburg, PA) for 48 hours. Incubation conditions contained 6.8 g/L fibrinogen, 100mM NaCl, and varied only in glucose concentration. For clot preparation, thrombin solution was prepared from Human α-Thrombin (ERL, Southbend, IN), 1M $CaCl_2$, and 50mM Tris Buffer. Stock Human α-Thrombin was diluted to 100 U/mL with 50mM Tris buffer, separated into 1 mL aliquots, and stored at -20°C prior to use. Fifteen minutes prior to the end of 48-hour fibrinogen incubation, a 100 U/mL Human α-Thrombin aliquot was thawed at room temperature and used to prepare 1 U/mL Human α-Thrombin, 100mM Calcium Chloride thrombin solution in a 1.5mL centrifuge tube.

Table 1: Volume of materials necessary for successful LSM 880 imaging of 0.0mM, 6.0mM, and 10.0mM glucose clots.

	Glucose Incubation Concentration		
Incubation Glucose Concentration	**0.0mM**	**6.0mM**	**10.0mM**
Total Incubation Volume	**100 µL**	**100 µL**	**100 µL**
FIB 3	**61.2 µL**	**61.2 µL**	**61.2 µL**
Alexa Fluor 488 Conjugate	**6.8 µL**	**6.8 µL**	**6.8 µL**
5M NaCl	**2 µL**	**2 µL**	**2 µL**
Final TGDI Concentration	**N/A**	**20mM**	**33.33mM**
TGDI Volume	**N/A**	**30 µL**	**30 µL**

Slide Preparation. Lifted platforms (Figure 15) were prepared to maintain fibrin clot structures by stacking labeling tape 20 mm apart on sterile glass microscope slides; five pieces of adhesive were used to create each side of the platform and the space aside the platform was used to load polymerized clots. For clot polymerization, 20 µL of an incubated fibrinogen solution and 20 µL

of the prepared Human α-Thrombin solution (1:1 dilution) were added to a clean 1.5 mL centrifuge tube, (a polymerization tube), and were pipette mixed several times to homogenize polymerization. From the resulting 40 μL solution, 30 μL of homogenized solution containing 3.4 g/L fibrinogen, 0.5 U/mL Human α-Thrombin, and specified amounts of glucose were then immediately transferred to the sample loading area. Five minutes after transferring the polymerization solution to the microscope slide, a 22 mm square transparent cover slip was placed over the sample to seal the sample loading area, limit air exposure, avoid contamination, and minimize dehydration during polymerization. Slides were placed in a microscope slide box and allowed to polymerize for 2 hours prior to imaging. A schematic (Figure 16) is provided to clarify the transfer of solutions for this described protocol.

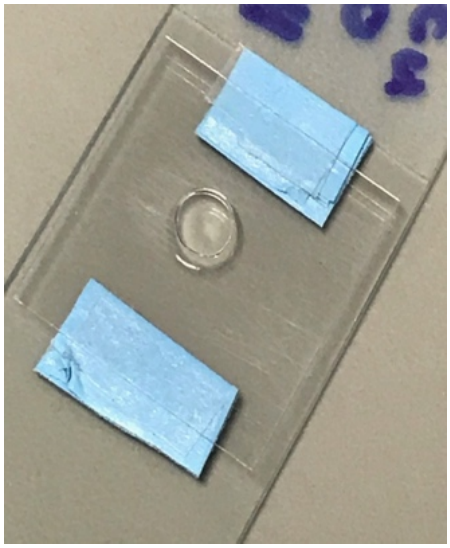

Figure 15: Lifted platforms were used to maintain fibrin gel's native structure and protect clots from contamination during the two-hour polymerization period.

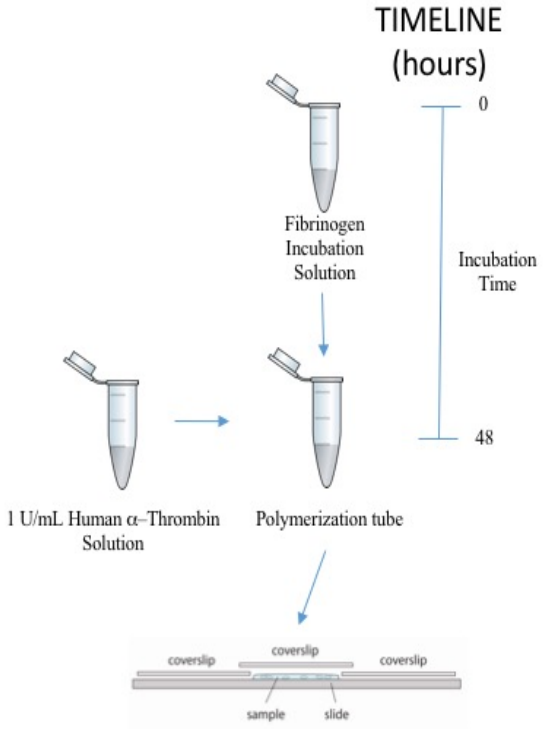

Fibrin Clot with 3.4 mg/mL fibrinogen, 0.5 U/mL Thrombin

Figure 16: A schematic for the transfer of solutions for fibrin clot polymerization.

Laser Scanning Microscopy Parameters. Fibrin clots were imaged using laser scanning confocal microscopy (LSCM) on a LSM 880 with 20X Plan-Apo/0.75 NA and DIC capability

(Ziess, Oberkochen, Germany). For each glucose condition, 0.0mM, 6.0mM 10.0mM, a minimum of nine z-stacks were collected to represent the imaging condition; three representative locations were selected to collect z-stacks from polymerized clots. A minimum of 60 slices were collected for each z-stack at 0.5 μm and 2X zoom.

Colorimetric Glucose Assay Procedure. A Colorimetric Glucose Assay (Cayman Chemical, Ann Arbor, MI) was performed on an EPOCH Microplate Spectrophotometer (BioTek, Winooski, VT) to quantify fibrinogen glycation. A sodium phosphate assay buffer (SPAB), a 1000 mg/dL glucose standard, and a lyophilized enzyme mixture were provided in the assay kit; these materials were prepared separately and used in colorimetric glucose assay protocol. SPAB was prepared by mixing the provided 10 mL of 250 mM sodium phosphate with 40 mL of HPLC water. The enzyme mixture was prepared by reconstituting the provided lyophilized vial with 6 mL of the SPAB. The glucose standard of 100 mg/dL was prepared by diluting the provided 1000 mg/dL glucose with SPAB; the standard curve was built by further diluting the 100 mg/dL glucose standard with SPAB (Table 2) and running colorimetric glucose assay protocol.

Table 2: Volumes of SPAB and 100 mg/dL glucose standard used to build the standard curve.

Glucose (mg/dL)	Average Raw Abs @ 510nm	Corrected Average Abs @ 510nm	Standard Deviation	Standard Trial1	Standard Trial2
0	0.1480	0.0000	0.0020	0.146	0.15
2.5	0.2530	0.1050	0.0190	0.234	0.272
5	0.2665	0.1185	0.0245	0.242	0.291
7.5	0.4850	0.3370	0.0050	0.49	0.48
10	0.5535	0.4055	0.0045	0.558	0.549
15	0.8485	0.7005	0.0045	0.844	0.853
20	0.9135	0.7655	0.0985	1.012	0.815
25	1.0685	0.9205	0.1235	0.945	1.192

The colorimetric assay protocol (Figure 17) was conducted by adding 85 μL of SPAB, 15 μL of a homogenized standard, and 100 μL of colorimetric enzyme mixture to a well of a 96-

well microplate. The 96-well place microplate was incubated at 37°C for 10 minutes and absorbance was measured at 510nm on an EPOCH Microplate Spectrophotometer (BioTek, Winooski, VT). The protocol was repeated twice for each standard and fit to the absorbance readings.

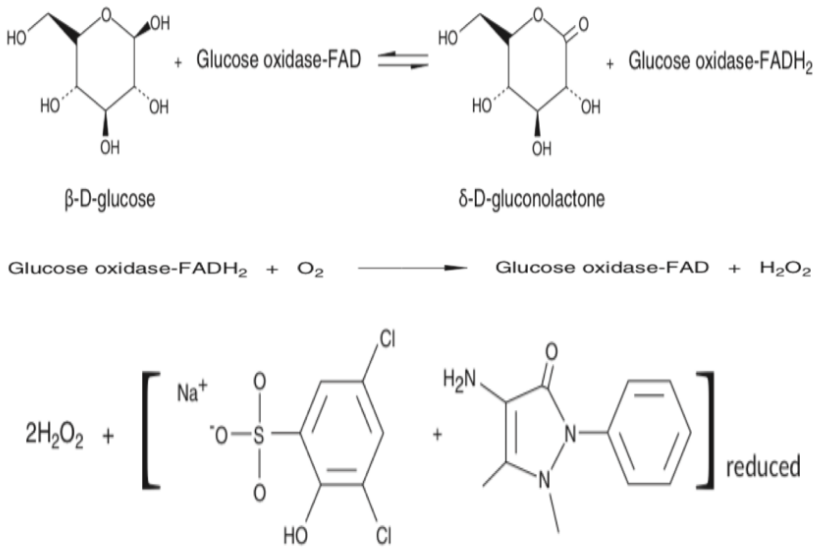

Figure 17: Reaction scheme of Colorimetric Glucose Assay.

The colorimetric glucose assay was conducted on glucose conditions 0.0mM. 6.0mM, and 10.0mM, containing 6.8 g/L FIB 3 Plasminogen, von Willebrand Factor and Fibronectin depleted, 100mM NaCl. Glucose concentration was integrated into incubation volumes via diluting 40mM glucose stock buffer; conditions were identical to LSM imaging conditions. After preparing glucose conditions, a portion was transferred to the 1.5mL centrifuge tube and diluted (1:4) with SPAB. The remaining glucose condition was placed in the 5L Isotemp Water Bath and incubated at 37°C for 48 hours for later use; only diluted samples were used in this colorimetric glucose assay protocol. The colorimetric glucose assay protocol was conducted immediately after sample dilution by adding 15 µL of homogenized sample, 85 µL of SPAB, and 100 µL of colorimetric enzyme mixture to a well of a 96-well place microplate. The microplate was

incubated at 37°C for 10 minutes and absorbance was read at 510nm on an EPOCH Microplate Spectrophotometer (BioTek, Winooski, VT). Five samples per condition were taken and three readings were collected from each sample to ensure homogeny and consistency between readings of a glucose sample. The same methodology was conducted on incubated glucose conditions at the end of the 48-hour incubation period. Zero and 48-hour absorbance readings were used in subsequent calculations using the change in free glucose over 48 hours and presented in the quantifiable form of mol(glucose)/mol(fibrinogen).

Image processing. Image processing enhanced z-stack slices using multiple feature detection techniques of the Image Processing Toolbox in MATLAB (MathWorks, Natick, MA) [172]. Geometrical tubular elements were identified with the fibermetric function, which used multi-scale second order local structures or a "vesselness" measure of eigenvalues from a Hessian pixilated matrix, to detect tubular structures [169]. This function accurately identified tubular structures, but also filtered out areas of dense fiber overlap; a mean filter function was used to identify densely populated fiber areas within each original z-stack slice. These two pre-processing techniques were combined into a single preprocessed image and used in subsequent segmentation methods. Specifically, houghpeak (Hough Transform) and houghline (Hough Line) functions were applied to generate Cartesian line segments through the center of tubular structures to represent detected fibrin fiber [7, 169, 170].

Fibrin Clot Characteristic Algorithms. Fibrin fiber overlap, fibrin fiber length, fiber matrix porosity, and fractal dimension were computed to determine mean variations. Fibrin fiber overlap was calculated by computing the number of overlaps (intersections) for each fibrin fiber. Fibrin fiber length was calculated by computing the length of each Hough Line; fiber length was measured in pixels and presented in a more tangible length measurement, microns. Fiber matrix

porosity was calculated by dividing the number of "on" pixels by the total number of pixels for each pre-processed 2-D slice. Fractal dimension was calculated using the Hausdorff box-counting method [173-175].

Statistical Analysis. Microsoft Excel was used for data management and pre-processing and statistical analysis was performed using SAS 9.4 (SAS, Cary, North Carolina) at a 95% confidence interval [176].One-way ANOVAs with the Tukey HSD post hoc test were performed on characteristic measurements and fibrinogen glycation from incubated 0.0mM, 6.0mM and 10.0mM glucose images (Appendix B).

4.2 Results

Representative images for the glucose concentrations (Figure 18) illustrated variations in fibrin fiber structure characteristics. These images were used as a reference when discussing characteristic differences from feature detection outputs. While not physiologically relevant, the 0.0mM condition was selected to provide a baseline comparison to glucose containing conditions.

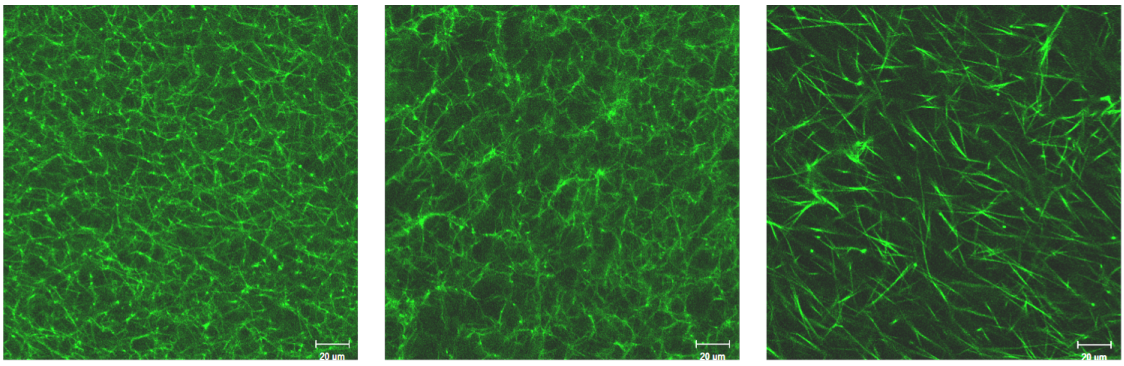

Figure 18: Representative images of the (A): 0.0mM, (B): 6.0mM, and (C): 10.0mM glucose conditions obtained from a LSM 880 at 20X Plan-Apo/0.75 NA and DIC capability with 2x optical zoom.

Fibrin Clot Characteristics. Fibrin clot characteristics for the three glucose concentration levels are summarized in Table 3. The number of samples (N), means, and standard deviations revealed

significant differences ($p < 0.0001$) for clot structure characteristics. Fibrin fiber overlap and fractal dimension were not significant between the 0.0mM and 6.0mM measurements, but both conditions were significantly different from 10.0mM glucose.

Table 3: Fibrin clot structure parameter outputs for the three glucose conditions.

Variables	0.0mM	6.0mM	10.0mM
N	843	857	643
Overlap Mean	14.67	14.29	10.33
Overlap STD.P	4.85	2.33	2.31
Length Mean (μm)	24.96	24.31	22.88
Length STD.P	1.77	0.89	1.04
Porosity Mean (%)	75.57	77.10	86.37
Porosity STD.P	4.94	3.81	3.68
Fractal Dimension	1.754	1.736	1.632
Fractal STD. P	0.039	0.037	0.055

Fibrin Fiber Overlap Variation with Glucose Concentration. The 0.0mM condition resulted in the highest fibrin fiber overlap average (14.67) and this value decreased as glucose concentration increased (Figure 19). While this trend was also observed as glucose concentration increased from 0.0mM to 6.0mM glucose (14.29), mean fibrin fiber overlap between the 0.0mM and 6.0mM glucose conditions was not significantly different. However, the means for fibrin fiber overlap measured in the 0.0mM and in the 6.0mM glucose conditions were found to be significantly different ($p < 0.0001$) from the10.0mM glucose condition (10.33).

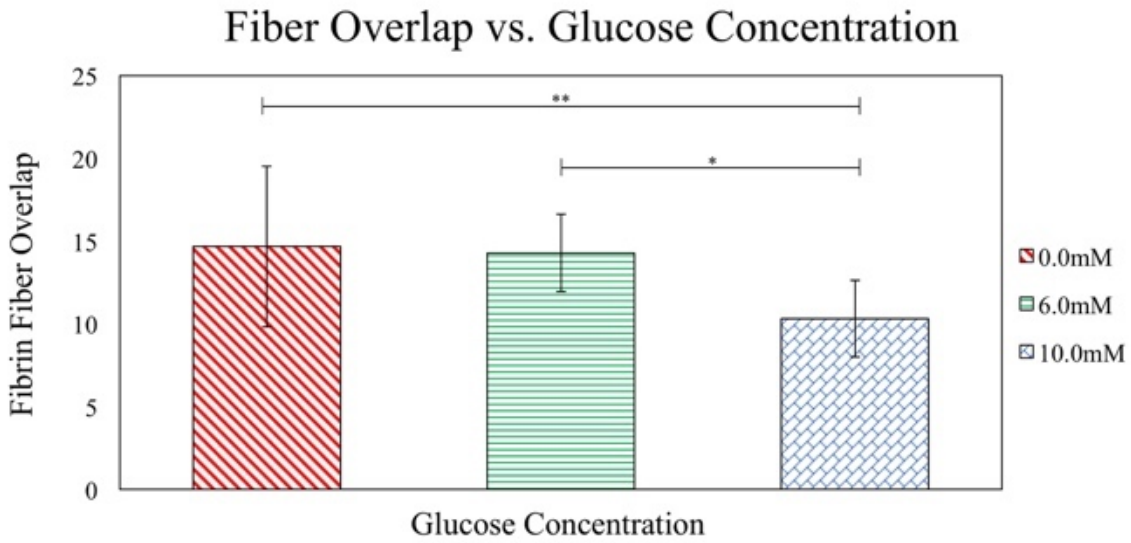

Figure 19: Fibrin fiber overlap averages for the 0.0mM (N = 843), 6.0mM (N = 857), 10.0mM (N = 643) glucose incubation concentrations with standard deviation error bars. Statistical significance: * p < 0.0001, ** p < 0.0001.

Fibrin Fiber Length Variation with Glucose Concentration. Longitudinal variations in Hough Lines were used to quantify fibrin fiber length. The highest average fibrin fiber length (Figure 20) was measured in the 0.0mM condition (24.96 μm) and decreased as glucose concentration increased; fibrin fiber length average also decreased from the 6.0mM (24.31 μm) to 10.0mM condition (22.88 μM). Glucose concentration had a significant effect on fibrin fiber length for the three glucose conditions.

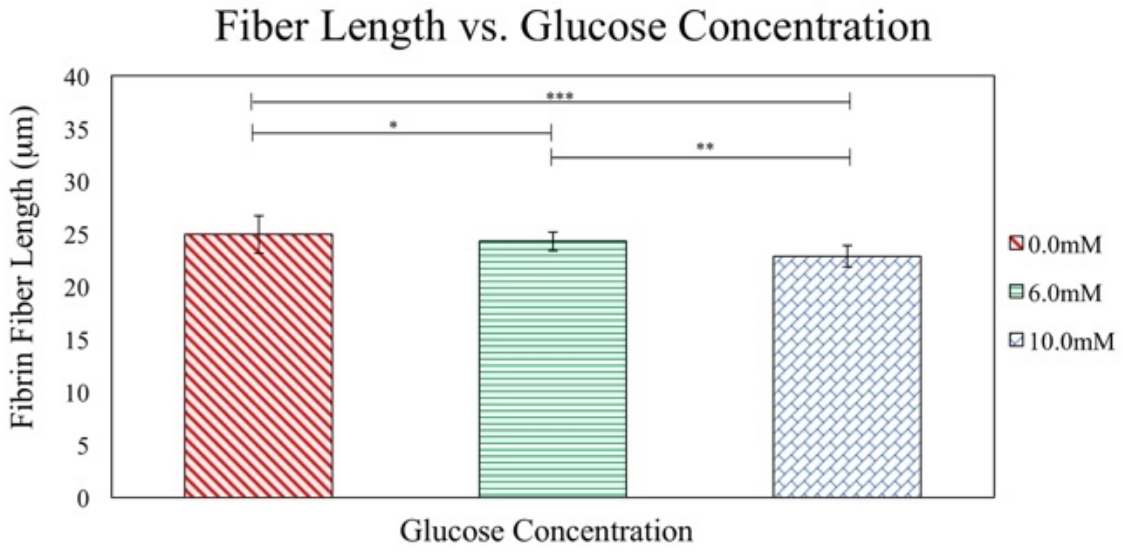

Figure 20: Fibrin fiber length averages converted into microns for the 0.0mM (N = 843), 6.0mM (N = 857), 10.0mM (N = 643) glucose incubation concentrations with standard deviation error bars. Statistical significance: * $p < 0.0001$, ** $p < 0.0001$, *** $p < 0.0001$.

Fibrin Matrix Porosity Variation with Glucose Concentration. Fibrin matrix porosity (Figure 21) increased as glucose concentration increased. Highest porosity was seen in the 10.0mM glucose condition (86.37%), with decreases revealed for both the 6.0mM condition (76.10%), and the 0.0mM condition (75.57%). Glucose concentration affected fibrin matrix porosity as evidenced by mean significant differences ($p < 0.0001$) between all three glucose concentrations.

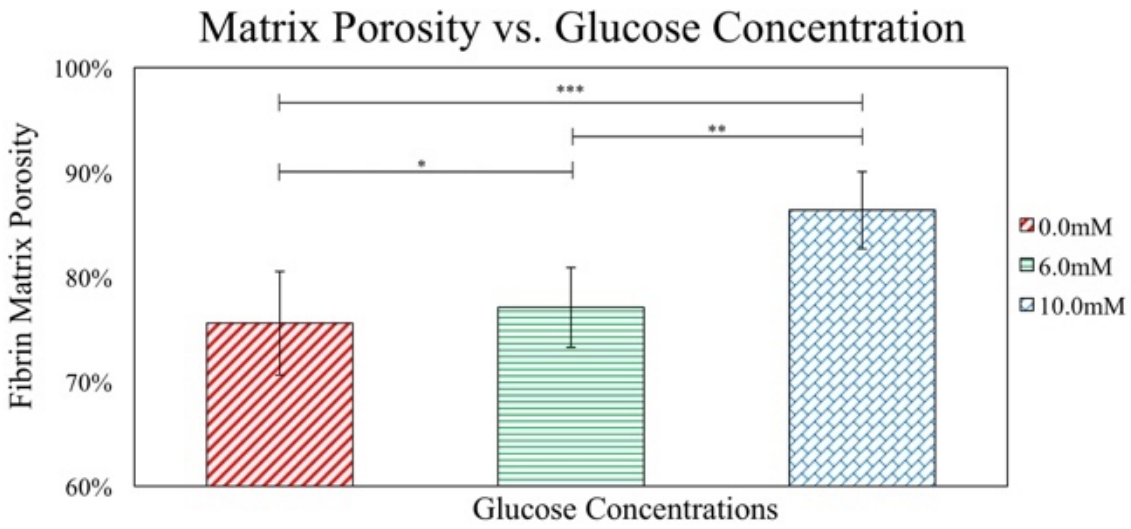

Figure 21: Fibrin matrix porosity averages for the 0.0mM (N = 843), 6.0mM (N = 857), 10.0mM (N = 643) glucose incubation concentrations with standard deviation error bars. Statistical significance: * p < 0.0001, ** p < 0.0001, *** p < 0.0001.

Fractal Dimension Variation with Glucose Concentration. Fractal dimension (Figure 22) decreased as glucose concentration increased. With the lowest fractal dimension observation in the 10.0mM glucose condition (1.632), fractal dimension increased in the 6.0mM condition (1.736) and was highest in the 0.0mM condition (1.754). Mean fractal dimension did not differ significantly between the 0.0mM and 6.0mM glucose conditions, but both were found to be significantly different ($p < 0.0001$) from the 10.0mM condition.

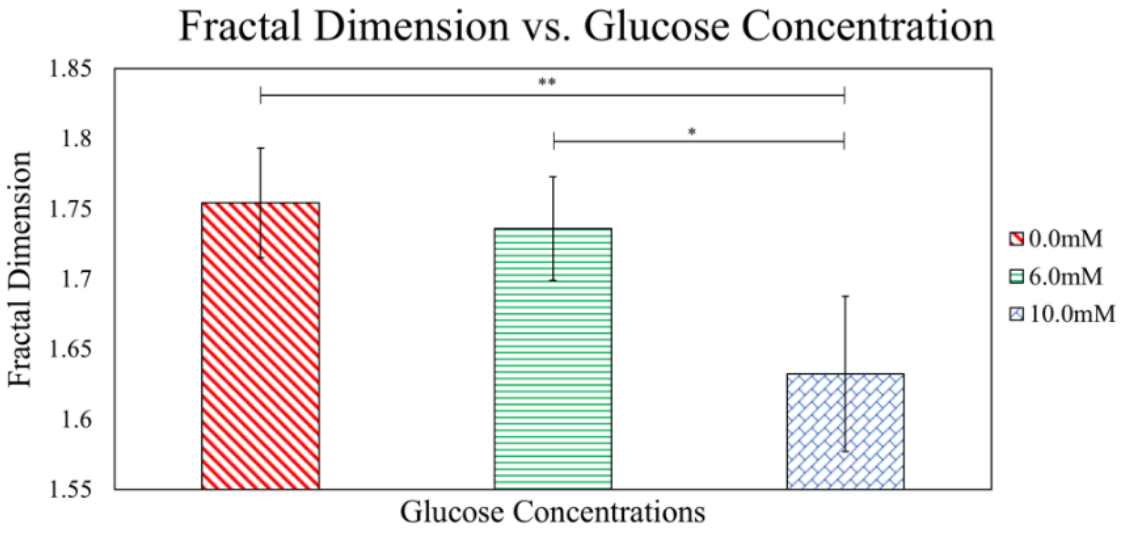

Figure 22: Fractal Dimension averages for the 0.0mM (N = 843), 6.0mM (N = 857), 10.0mM (N = 643) glucose incubation concentrations with standard deviation error bars. Statistical significance: * p < 0.001 and ** p < 0.0001.

Fibrinogen Glycation Independent of Fibrinogen Concentration. The colorimetric glucose assay evaluated the effect of glucose concentration on fibrinogen glycation. A standard curve (Figure 23) from known stock concentrations of diluted glucose standards was used to calculated free glucose sample conditions. The standard curve linearly fit to absorbance at 510nm (R^2 = 0.9703).

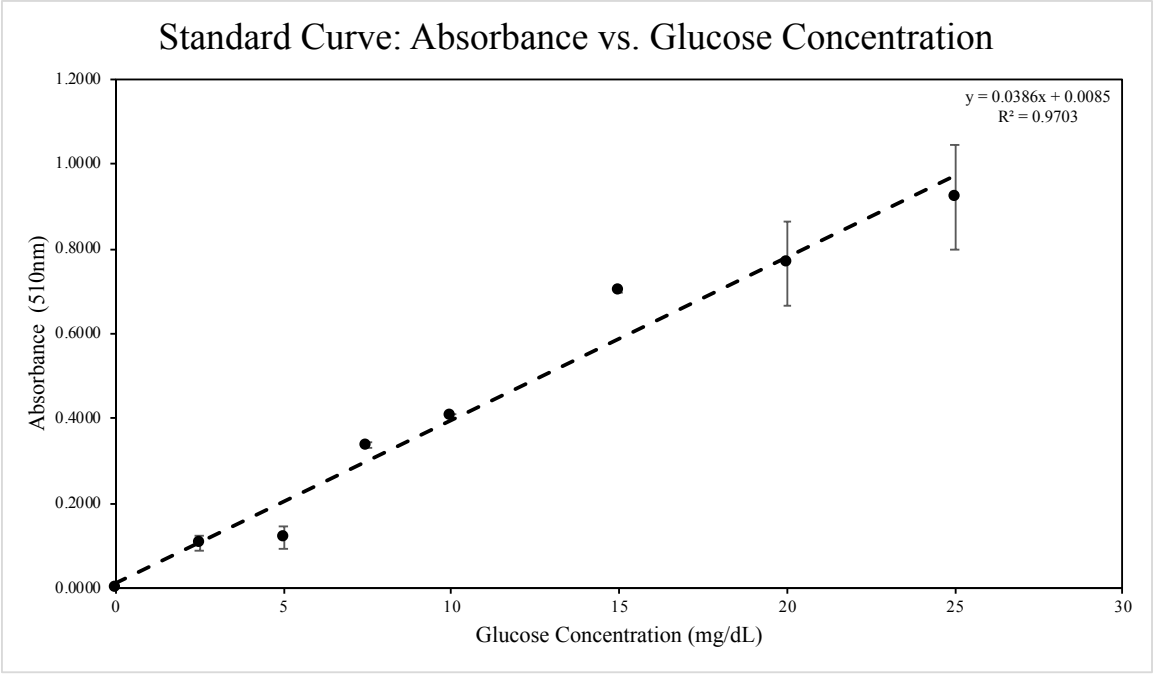

Figure 23: Standard Curve from colorimetric glucose assay. The curve was developed by plotting the measured absorbance at 510nm after 10 minutes of incubation vs. each known concentration of glucose.

Colorimetric glucose assay measurements (Table 4) were collected to quantify fibrinogen glycation. At T=0, free glucose concentration measured 0.042mM, 5.476mM, and 9.104mM for the 0.0mM, 6.0mM, and 10.0mM conditions, respectively. After 48 hours of incubation, mean free glucose concentration decreased in all three glucose conditions; free glucose concentration measured 0.012mM, 5.328mM, and 8.116mM for the 0.0mM, 6.0mM, and 10.0mM conditions, respectively. The change in free glucose was used to calculate fibrinogen glycation over 48 hours of incubation at 37°C. The highest glycated fibrinogen concentration, 4.942 $mol_{glucose}/mol_{fibrinogen}$, was found in the 10.0mM condition and decreased with decreasing glucose concentration. Fibrinogen glycation concentration measured 0.743 $mol_{glucose}/mol_{fibrinogen}$ for the 6.0mM condition and 0.154 $mol_{glucose}/mol_{fibrinogen}$ for the 0.0mM condition. Glycated fibrinogen concentration, 0.154 $mol_{glucose}/mol_{fibrinogen}$, for the 0.0mM condition is effectively zero because: 1) the associated error, 0.49, was greater than the measured value at T =0 and 2) the colorimetric

glucose assay lower level of detection (0.013mM) was lower than the free glucose concentration (0.012mM) at T=48.

Table 4: Colorimetric glucose assay measurements used to quantify fibrinogen glycation after 48-hour incubation.

Variables	0.0mM	6.0mM	10.0mM
Free Glucose @ T = 0 (mM)	0.0424	5.476	9.104
Free Glucose @ T = 0 STD.P	0.049	0.122	0.200
Free Glucose @ T = 48 (mM)	0.012	5.328	8.116
Free Glucose @ T = 0 STD.P	0.059	0.347	0.431
Δ in Free Glucose (mM)	0.031	0.149	0.989
Fibrinogen Concentration (mM)	0.200	0.200	0.200
Glycation ($mol_{glucose}/mol_{fibrinogen}$)	0.154	0.743	4.942
Glycation STD. P	0.011	0.047	0.063

The average of the initial free glucose, the free glucose after 48 hours, and glycated fibrinogen (Figure 24) were calculated from 15 sample trials per condition. Although the zero hours absorbance readings were linear with glucose concentration, the 48 hours readings were not. Fibrinogen glycation over 48 hours was also not a linear function of glucose condition as glycated fibrinogen in the 0.0mM and 6.0mM conditions were significantly lower than the 10.0mM condition. Results from a one-way ANOVA found glucose concentration to significantly ($p < 0.0001$) affect glycated fibrinogen concentration.

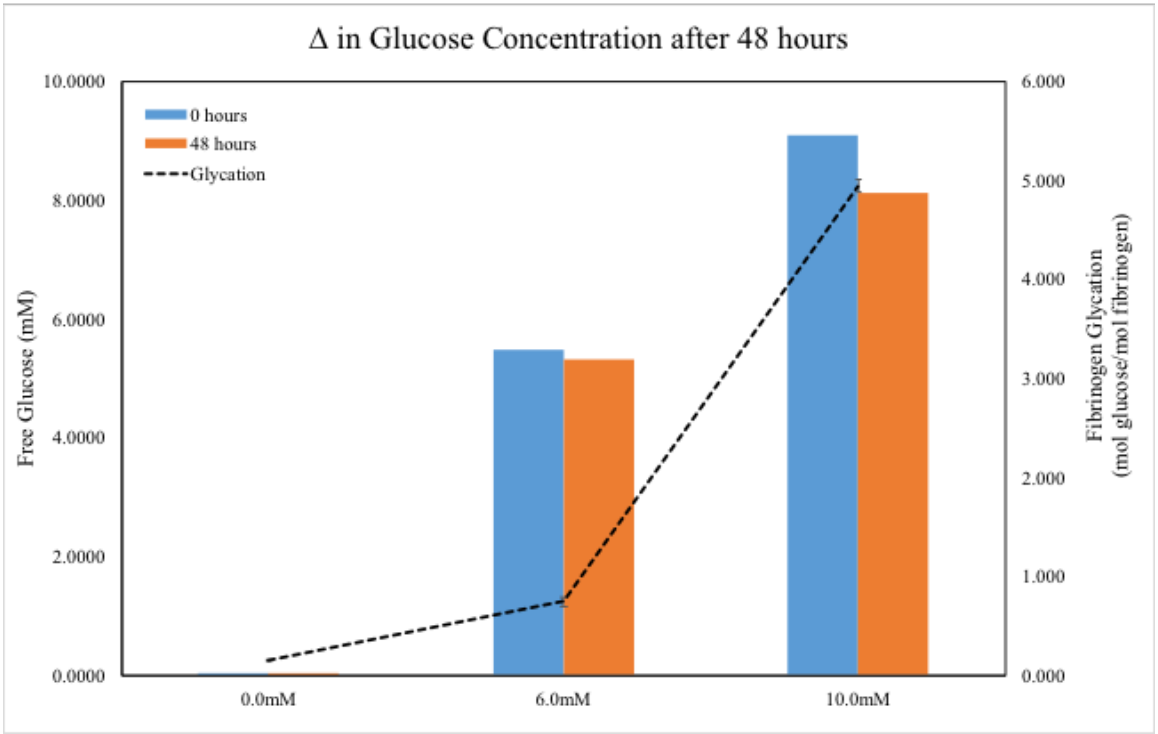

Figure 24: Change in free glucose and fibrinogen glycation after 48 hours of incubation at 37°C.

4.3 Discussion

This study had two main aims. The first was to evaluate the effect of glucose concentration of fibrin clot characteristics at three glucose concentrations. The second, which has not been experimentally tested before and which significantly contributes to the experimental literature to-date, was to conduct fibrinogen glycation measurement in a controlled *in vitro* environment in hopes of elucidating that hyperglycemia increases fibrinogen glycation, alters clot characteristics, and influences clot behavior in DM.

Experimentally, the presented methodology was able to visualize fibrin clot structure characteristics for three glucose concentrations in a controlled *in vitro* fibrinogen system. The use of a 10% dye of fibrinogen concentration provided an effective balance of florescent and non-florescent fibrinogen; a higher percentage of total fibrinogen may have resulted in image

saturation and the inability to distinguish fibrin fibers, while a lower dye percentage may have resulted in under-detection or indistinguishable variation in fibrin fiber characteristics. The selection of a 0.0mM glucose condition (although not physiologically relevant) provided a baseline comparison to the 6.0mM and 10.0mM glucose conditions.

Fibrinogen glycation was suspected to influence changes in fibrin clot characteristics and promote macrovascular disease, but quantification of fibrinogen glycation under a consistent fibrinogen concentration *in vitro* is novel to this experimentation. The colorimetric glucose assay was able to measure changes in free glucose and calculate fibrinogen glycation within range of previously conducted *in vivo* studies [114, 177, 178]. Often, glycated protein assays are used to measure glycated fibrinogen during clinical examination, but the colorimetric glucose assay was selected for this study because: 1) the glycated protein assay is not specific to fibrinogen; and 2) fibrinogen is a large protein; when assay reactions are not specific to that protein, the large protein size of fibrinogen adds additional accuracy concerns. The glycated protein assay uses a generic protease to generate protein fragments before measuring glycation, and so, inconsistent cleavage of fibrinogen could explain the lower glycation measurements in this study in comparison to clinical results. Unfortunately, however, colorimetric glucose assay protocol is not possible *in vivo* because fibrinogen is exposed to glucose prior to measurement and no glycation baseline can be measured for comparison. Without more information of all glucose binding sites to fibrinogen, the glycated protein assay may be the best method currently available to quantify glycated fibrinogen *in vivo*.

Secondly, the presented computational methodology was able to successfully distinguish fibrin clot characteristics that appeared visually different in the three glucose conditions. The fibermetric function calculated multi-scale second order local structures and was found to be an

effective pre-processing approach when coupled with a mean filter function. Both functions were necessary to detect the local likelihood of vessels for densely populated fiber areas and feature detection methods that do not consider local geometry or account for highly populated local fibrin areas may result in less accurate recognition of tubular features. Overall, the ability of the presented computational methodology to detect fibrin matrix features for densely populated fiber areas and multiple size ranges may provide advantages in future *in vivo* experimentation of fibrin clot characteristics.

Fibrin fiber overlap was used as a quantitative reference to examine the connective behavior of detected fibrin fiber aggregates. The lack of significant difference found between the 0.0mM and 6.0mM glucose conditions could be explained by differences in fiber length outputs for these conditions. Since the average length of the 6.0mM glucose condition was shorter than the 0.0mM condition, the shorter fibers are less likely to overlap with other randomly oriented shorter fibers in the 6.0mM condition. While another study has shown that glucose concentration increased fibrin fiber overlap, fibrin fiber overlap at glucose concentrations higher than 10.0mM also decreased in this study; different computational methodologies, different macromolecule concentrations (thrombin, fibrinogen, and, FXIII, etc.), and different image magnifications were conducted, so results may not be comparable [7]. Future study to further examine the effect of glucose concentration and other macromolecules like FXIII on fibrin fiber overlap are needed.

Fibrin fiber length was measured to confirm dehydration and did not compromise results. Fiber length measurements are all in agreement with fibrin fiber length averages (23 +/- 9 μm) from previous studies and confirm that native fibrin clot structures were maintained [179, 180]. While fiber length decreased with increasing glucose concentration and was significantly different between glucose groups, it is difficult to makes claims of the true effect of glucose

concentration on fibrin fiber length here because results are based on two-dimensional images of three-dimensional structures. The effect of glucose concentration on fibrin fiber length could be made by developing three-dimensional representations of fibrin matrixes, but the z-stack slice distance (0.5 μm) is too large to accurately connect fiber diameters (0.1 μm) in adjacent z-stack slices.

Traditionally, the term porosity indicates the amount of spaces or holes through which fluid can flow. Since fibrin matrix porosity represents the proportion of "on" pixels and is presumed to be a measure of clot permeability, and porosity measurements in this study actually indicate fibrin fiber density. Assuming samples were homogenized with equal amounts of fibrinogen (unique to this study), higher porosity measurements indicate more densely compacted formed fibrin fibers. Many studies have presented data on the effects of protein glycation on fibrin fiber density, clot stability, resistance to lysis, and their influences of clotting risk, but this is the first study to our knowledge that examines the effect of glucose concentration on fibrin fiber density in a controlled *in vitro* fibrinogen system [46, 109, 113-117, 181, 182]. In clinical examinations, DM's defining characteristic of resting hyperglycemia is often used to justify changed fiber characteristics, clot stability, and thrombus behavior. However, the extent of hyperglycemia's influence on unstable and spontaneous clot formation in the diabetic patient remains highly debated due to many factors including hyperfibrinogenemia, hyperinsulinemia, dyslipidemia, hypertension, obesity, decreased fibrinolysis, endothelial dysfunction, and changed platelet aggregability which are known to influence thrombus formation present themselves simultaneously [54, 62, 64, 65, 85, 87-89, 113, 183]. For example, fibrinogen concentration, an established independent risk factor for CVD, regardless of vascular event history, has shown to influence fibrin clot structure [105-108, 184]. In a study of hyperfibrinogenemic mice, fibrin

fiber characteristics showed significant changes, quicker vessel occlusion, increased fibrin mass, and poor fibrinolytic behavior when compared non-hyperfibrinogenemic controls [185]. As such, if fibrinogen concentration is consistently higher in diabetic patients and apparently variable across patients, the effects of hyperglycemia on DM and on fibrin(ogen) conversion, fibrin fiber formation, clot stability, and thrombus behavior have yet to be thoroughly examined *in vivo* [186]. As diabetics consistently form more compact clots, fibrin fiber density measurements, independent of fibrinogen concentration, provide further evidence supporting hyperglycemia's influences on fibrinogen glycation that affect fibrin clot morphology.

Measurement of fractal dimension (d_f) is becoming increasingly studied as a potential biomarker of macrovascular risk with many studies demonstrating how changes in d_f relate to changes in thrombus mass [187-190]. However, the majority of these analyses use Scanning Electron Microscopy (SEM) images which makes it difficult to compare this approach with LSM; a higher d_f is typically associated with denser, at risk, fibrin clot structure, but a reverse trend was seen with the LSM methodology. Examining the relationship between thrombin concentration and d_f with constant fibrinogen concentration, Hawkins et al. (2012) found LSM clots were qualitatively different in clot architecture at different thrombin concentrations and increased in d_f with increasing thrombin concentration [191]. In comparison with our findings, this trend suggests increased glucose concentration actually slows clotting time to produce denser fibrin fibers as the 10.0mM condition produced the densest formed fibers and lowest d_f. Additionally, although not conducted under a consistent fibrinogen concentration, kinetic measurements of fibrinogen polymerization time found that stable thrombus formation was significantly higher (6.6 vs. 7.3 minutes, $p < .05$) in hyperglycemic conditions [192], and under other experimental investigation increasing glucose concentration was shown to drastically

prolong clot formation time [6]. Therefore, d_f measurements from LSM studies in which a dye percentage is applied may better explain clotting rate. While hyperglycemia is associated with enhanced thrombin formation, platelet activation, and resistance to lysis, it is likely the combination of increased fibrinogen and thrombin concentrations drive clot formation. However, it is hyperglycemia, via fibrinogen glycation, that prolonged clotting time and caused denser fiber fibers to form.

4.4 Conclusion

Algorithm outputs coupled with statistical analysis found generalized findings between glucose concentration and fibrin clot structure characteristics. This supports *in vivo* findings that hyperglycemia alters fibrin clot structure in diabetic patients, independent of fibrinogen concentration. Fibrin fiber length measurements were consistent with previous conducted studies and confirmed that the native structure of imaged conditions was maintained. Matrix porosity found glucose concentration increased fibrin fiber density. Fractal dimension decreased with increasing glucose concentration supporting literature that suggests glucose concentration slows thrombus time; increased fibrinogen and thrombus concentrations in DM drives clot formation, but produces thrombi of increased fiber density. Fibrinogen glycation was found to be highest in the mimicked hyperglycemic condition (10.0mM) and had a pronounced effect with increased glucose concentration. To our knowledge, this is the first study to examine the effects of glucose concentration on fibrinogen glycation independent of fibrinogen concentration using a colorimetric glucose assay. Overall, imaging and glycation results advocate that hyperglycemia increases fibrinogen glycation and changes morphological clot characteristics. Significant differences in measured fibrin clot structure parameters at three glucose concentrations present a proof of concept for the application of LSM imaging to characterize fibrin clot structure. As

significant differences in clot structure characteristics were distinguishable, this technique could provide medical professionals with an alternative diagnostic tool for evaluation of clotting risk if adapted to human plasma.

CHAPTER 5: NITRIC OXIDE RELEASE INTEGRATION

5.1 Materials and Methods

NO experimentation analyzed the efficacy in utilizing NO mechanisms to limit clot formation in hyperglycemic environments. Specifically, the effects of polymer and nitric oxide (NO) on clot morphology were examined using NO-releasing polymer, SNAP. Clot conditions contained the same glucose concentrations used in the original glucose study (0.0mM, 6.0mM, and 10.0mM) FIB 3 Plasminogen, von Willebrand Factor and Fibronectin depleted (ERL, Southbend, IN), and fibrinogen from Human Plasma Alexa Fluor 488 Conjugate (Fisher Scientific, Pittsburg, PA). LSM data were collected under the same imaging parameters, image processing techniques, and were compared to original glucose condition findings. Two durations were selected for NO examination, 2hr and 48hr, and only differed in polymer exposure (SNAP and NAP). Specifically, 12 new imaging conditions (0.0mM2hrNAP, 6.0mM2hrNAP, 10.0mM2hrNAP, 0.0mM2hrSNAP, 6.0mM2hrSNAP, 10.0mM2hrSNAP, 0.0mM48hrNAP, 6.0mM48hrNAP, 10.0mM48hrNAP, 0.0mM48hrSNAP, 6.0mM48hrSNAP, 10.0mM48hrSNAP) were conducted to investigate polymer and NO release on pre-glycated fibrinogen for two hours and in competition with glucose over 48 hours.

S-Nitroso-N-acetylpenicillamine Synthesis. SNAP was integrated into a biocompatible polymer to examine NO flux effects on clot polymerization. SNAP synthesis was required for polymer integration; equimolar NAP (Sigma Aldrich, St. Louis, Missouri), sodium nitrite, and methanol were mixed with 1M HCl/H_2SO_4 for 15 minutes and cooled in an ice bath for 6 hours [193]. Using a modified protocol, SNAP was purified by washing with water/acetone/diethyl

ether before collection. Purified SNAP was collected via vacuum filtration for use in a 10 wt% SNAP polymer coating during LSM examination. 10 wt% SNAP was selected for polymer integration to meet a NO release profile similar to physiological endothelial release over 48 hours.10 wt% N-acetyl-D-penicillamine (NAP) was used as a comparison to 10 wt% SNAP polymer because NAP is typically used to examine NO specific effects, SNAP was synthesized from NAP, and NAP decomposes similarly to SNAP, albeit without NO release.

Polymer Tube Coating. 10 wt% SNAP polymer was prepared by dissolution in THF; 110 mg/mL CarboSil 2080A (DSM, Exton, PA) was dissolved with 10 wt% SNAP. CarboSil was selected for integration to examine NO specific actions due to its unique thromboresistance, biostability, protein adhesion, and NO-release behavior for biomedical applications [194]. 10 wt% NAP polymer was prepared in identical fashion, but 10 wt% NAP was used during dissolution in lieu of 10 wt% SNAP. NAP/SNAP polymer coating protocol was then performed with 10 wt% NAP/SNAP polymer by transferring 1 mL of bulk solution to 1.5 mL centrifuge tubes. Tubes were inverted and air-dried under a fume hood to remove excess and produce even polymer coatings. Tubes were labeled appropriately and stored at -20°C. Note: 1.5 mL centrifuge tubes were coated from homogenized bulk polymer solutions to reduce NO variance between individual tubes.

NO Polymer Exposure Experimentation. Two NO exposure conditions were selected for 10 wt% NAP/SNAP tube experimentation: 1) two-hour exposure, 2hrSNAP, post 48-hour incubation and 48-hour NO exposure, 48hrSNAP, simultaneously with glucose incubation. For the two-hour NO exposure condition, glucose conditions (0.0mM, 6.0mM, and 10.0mM) were incubated in clean 1.5 mL centrifuge tubes (without polymer coating) at 37°C in a 5L Isotemp Water Bath (Fisher Scientific, Pittsburg, PA) for 48 hours. Total volumes were then transferred

to 10 wt% polymer tubes and incubated for an additional two hours before polymerization. The two-hour NO exposure condition was compared to the original glucose condition because it only differed in an additional two hours of incubation exposure to 10 wt% NAP/SNAP post initial incubation and aimed to analyze the effect of limited NO exposure on pre-glycated fibrinogen. For 48 hour NO exposure, glucose conditions (0.0mM, 6.0mM, and 10.0mM) were incubated directly in 10 wt% NAP/SNAP polymer tubes in a 5L Isotemp Water Bath (Fisher Scientific, Pittsburg, PA) at 37°C for 48 hours. 48-hour NO exposure conditions were compared to original glucose conditions to examine the competing effects of fibrinogen glycation and NO release. All incubation conditions were polymerized using equal concentration thrombin solution from the original glucose study.

Clot Preparation Protocol. For clot polymerization, thrombin solution was prepared from Human α-Thrombin (ERL, Southbend, IN), 1M $CaCl_2$, and 50mM Tris Buffer using 1 mL aliquots of dilute 100 U/mL Human α-Thrombin. Aliquots were further diluted to 1 U/mL Human α-Thrombin, 100mM Calcium Chloride for thrombin solution preparation; thrombin solution preparation matched glucose study clot preparation protocol. New fibrin clot conditions were polymerized on clean microscope slide with lifted platforms by adding 20 μL of incubated fibrinogen solution and 20 μL of thrombin solution to clean 1.5 mL centrifuge tubes. Solution was then homogenized via pipette mixing. 30 μL of the resulting polymerizing solution was then transferred immediately to the sample loading area. Five minutes after transferring polymerization solution to the microscope slide, a 22 mm square transparent cover slip was placed over the sample to seal the sample loading area, limit air exposure, avoid contamination, and minimize dehydration during polymerization. Samples were placed in a microscope slide box and allowed to polymerize for 2 hours prior to LSM imaging.

LSM Imaging. Fibrin clots were imaged using LSCM on a LSM 880 with 20X Plan-Apo/0.75 NA and DIC capability (Ziess, Oberkochen, Germany). For each of the 12 new conditions, a minimum of nine z-stacks were collected to represent the imaging condition; for each condition, three representative locations were selected to collect z-stacks. A minimum of 60 slices were collected for each z-stack at 0.5 μm and 2X zoom.

Image processing. First, z-stacks images enhanced fibrin matrix aggregates using multiple feature detection techniques of the Image Processing Toolbox in MATLAB (MathWorks, Natick, MA) [172]. Geometrical tubular elements were identified with the fibermetric function, which used second order local structures or a "vesselness" measure of eigenvalues from a Hessian pixilated matrix, to detect tubular structures [169]. This function accurately identified tubular structures, but also filtered out areas of dense fiber overlap; a mean filter function was used to identify densely populated fiber areas within each original z-stack slice. These two pre-processing techniques were combined into a single preprocessed image and used in subsequent segmentation methods. For image segmentation, houghpeaks (Hough Transform) and houghlines (Hough Line) functions were applied to generate Cartesian line segments through the center of tubular structures; tubular structures were assumed to represent detected fibrin fibers [7, 169, 170]. Overall, fibrin fiber overlap and fibrin fiber length were calculated after Hough Line generation, while fiber matrix porosity was measured from pre-processed 2-D slices prior to segmentation.

Fibrin Clot Characteristic Algorithms. From z-stacks conditions, the same feature detection algorithms were used to identify fibrin clot structure characteristics. Fibrin fiber overlap was calculated by computing the number of overlaps (intersections) for each individual generated fibrin fiber. Fibrin fiber length was calculated by computing the length of each generated Hough

line; fiber length was later converted from pixels to a more tangible length microns measurement. Fiber matrix porosity was calculated by dividing the number of "on" pixels by the total number of pixels for each pre-processed 2D slice.

Statistical Analysis. Statistical analysis was performed using SAS 9.4 (SAS, Cary, North Carolina) at a 95% confidence interval and results were used to further support analytical findings [176]. Two-way ANOVAs with the Tukey HSD post hoc test were performed on LSM feature detection measurements to determine statistical significance; two-way ANOVA was required to quantify NO and glucose and interaction effects on the newly collected fibrin clot conditions.

Nitric Oxide Release Data. NO flux and accumulation profiles were developed to quantify NO release from 10 wt% SNAP films; NO release data was used to analyze fibrin clot characteristics measurements from LSM results. Specifically, NO flux and accumulation profiles were compared to non-NO releasing 10 wt% NAP polymer without NO release. NO flux and NO accumulation profiles were developed using photon data collected on a chemiluminescence Nitric Oxide Analyzer 280 (Sievers, Boulder, CO). For Nitric Oxide Analyzer use, 10 wt% SNAP films (1.00 cm^2) were immersed in sample vessels containing 4 mL of phosphate buffered saline (PBS) at 37°C. NO was continuously swept from the headspace into the chemiluminescence detection chamber with N_2 at a rate of 200 mL/min. Steady state NO flux measurements were collected at 0, 24, and 48 hour time points; NO flux was calculated by taking the difference of baseline and steady state fluxes averages and used for subsequent accumulation calculations. 10 wt% SNAP films (1.00 cm^2) were transferred to glass vials and stored at 37°C between collection points; PBS was replaced between data points. A total of nine 10 wt% SNAP

films were used to develop NO flux and release profile averages. One way-ANOVA was performed to determine the consistency of NO flux from 10 wt% SNAP.

Fibrinogen Fluorescence Assay. Fluorescence data was collected on glucose (0.0mM, 6.0mM, and 10.0mM) and 48 hour NO exposure (0.0mM48hrNAP, 6.0mM48hrNAP, 10.0mM48hrNAP 0.0mM48hrSNAP, 6.0mM48hrSNAP, 10.0mM48hrSNAP) conditions using a Synergy HTX Multi-Mode Microplate Reader (BioTek, Winooski, VT); incubation volumes were raised to 300 μL, but followed proportional concentrations of fibrinogen, dyed fibrinogen, and glucose from LSM conditions. A standard curve was prepared via series dilution of stock Fibrinogen from Human Plasma, Alexa Fluor 488 Conjugate with 50mM Tris buffer; fluorescence was measured twice and fit to known concentrations of fibrinogen from Human Plasma, Alexa Fluor 488 Conjugate. After 48-hour incubation, samples were homogenized for 10 seconds with a vortexer and 50 μL were used for fluorescence measurements; volume was transferred to a black 96-well microplate and read at 485/20, 528/20. Five samples were used to calculate dyed fibrinogen concentrations for incubation conditions with three trials coming from each sample. Two-way ANOVA was performed to quantify the effects of coating material, glucose concentration, and their interaction on dyed fibrinogen concentration.

5.2 Results

Results from the two-way ANOVA found significantly different mean differences for the twelve NO imaging conditions ($p < 0.0001$). However, LSM measurements between samples of polymerized NO exposure conditions were also found to vary significantly and were not analyzed for two reasons.

1. 10 wt% SNAP released variable amounts NO over 48 hour incubation; NO release data limited our ability to analysis 10 wt% SNAP specific effects on LSM

measurement. As NO flux was collected from 10 wt% SNAP films (separated from LSM incubation samples) LSM measurement cannot be correlated to the specific NO flux from LSM incubation tubes. However, NO flux was detected from all tested 10 wt% SNAP films and a baseline concentration of NO accumulate in incubations samples over 48 hours; NO likely had an addition influence on LSM measurements.

2. Despite not analyzing LSM measurements, polymerization did not occur (Figure 25) in four LSM 10 wt% conditions (10.0mM2hrSNAP, 0.0mM48hrSNAP, 6.0mM48hrSNAP, and 10.0mM48hrSNAP) that can be supported by fluorescence data. Both NAP and SNAP fluorescent data found 10 wt% polymer exposures to influence dyed fibrinogen concentration. While changing fibrinogen concentration provided explanation for the effects of 10 wt% SNAP (e.g., 0.0mM48hrSNAP) on LSM measurements, fibrinogen concentration is a known influence fibrin clot characteristics and further claims on glucose, NAP/SNAP, and polymer effects cannot be these LSM measurements.

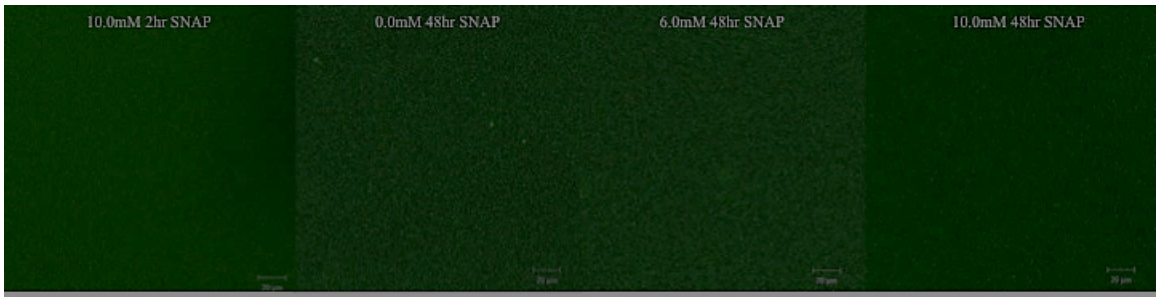

Figure 25: LSM 10 wt% conditions (Left to Right: 10.0mM2hrSNAP, 0.0mM48hrSNAP, 6.0mM48hrSNAP, and 10.0mM48hrSNAP) in which no fibrin fibers were detected during image processing and analysis.

NO Flux and Accumulation Profiles. Mean NO flux averages (Figure 26) for the 0, 24, and 48 hour time points of 10 wt% SNAP film were found to be 0.59l $\frac{mol^{-10}}{\min * cm^2}$, 0.184 $\frac{mol^{-10}}{\min * cm^2}$, and

0.153 $\frac{mol^{-10}}{\min*cm^2}$, respectively. However, one-way ANOVA found NO flux to be significant ($p < 0.001$) at each time point and insignificant ($p > 0.5$) between time points. Therefore, flux averages are not representative of individual 10 wt% SNAP NO release over 48 hours.

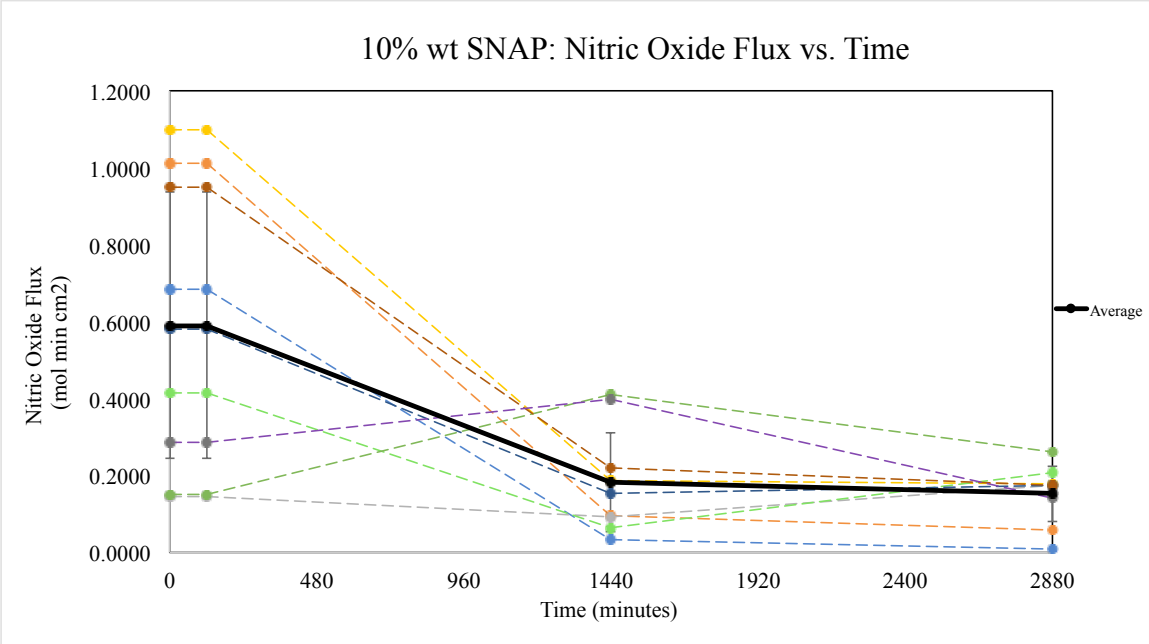

Figure 26: Nitric oxide flux from nine 10 wt% SNAP films with 0, 24, and 48 hours of incubation at 37℃. Flux average (solid black line) from the nine samples is not a representative of individual 10 wt% SNAP films.

Max/min fluxes for the 0, 24, 48 hour times points (max/min) measured 1.097/0.1435$\frac{mol^{-10}}{\min*cm^2}$, 0.4085/0.0347$\frac{mol^{-10}}{\min*cm^2}$, and 0.2597/0.0088$\frac{mol^{-10}}{\min*cm^2}$, but these extremes do not correspond to individual 10 wt% SNAP films. For example, NO flux of sample 2 (yellow) measured the highest (1.097$\frac{mol^{-10}}{\min*cm^2}$) of the nine samples at the 0-hour time period, but was not the maximum (0.4085$\frac{mol^{-10}}{\min*cm^2}$) at the 24-hour time point (0.0972$\frac{mol^{-10}}{\min*cm^2}$); the maximum NO flux at 24 hours corresponded to sample 6 (green). NO flux data (Table 5**)** demonstrates variable NO release from 10 wt% SNAP films over 48 hours.

Table 5: Output of total NO flux data from 10 wt% SNAP films over 48 hours at 37℃

	NO Flux mol*min^{-1}*cm^{-2}										
Time (minutes)	Sample 1	Sample 2	Sample 3	Sample 4	Sample 5	Sample 6	Sample 7	Sample 8	Sample 9	Average	STD.P of Averages
0	0.6844	1.0106	0.1435	1.0971	0.4153	0.1509	0.5813	0.9492	0.2846	0.5907	0.3477
120	0.6844	1.0106	0.1435	1.0971	0.4153	0.1509	0.5813	0.9492	0.2846	0.5907	0.3477
1440	0.0347	0.0972	0.0925	0.1847	0.0643	0.4085	0.1524	0.2218	0.3961	0.1836	0.1292
2880	0.0088	0.0563	0.1747	0.1782	0.2070	0.2597	0.1735	0.1747	0.1393	0.1525	0.0720

As NO flux was variable over 48 hours ($p > 0.5$), NO accumulation profiles, calculated from 10 wt% SNAP film NO flux, were also significantly different ($p > 0.5$) from each other. Mean NO accumulation averages (Figure 27) for the 0, 2, 24, and 48 hour time points of 10 wt% SNAP were found to be 0 $\frac{mol^{-10}}{cm^2}$, 70.890 $\frac{mol^{-10}}{cm^2}$, 824.279 $\frac{mol^{-10}}{cm^2}$, and 1285.775 $\frac{mol^{-10}}{cm^2}$, respectively, but these averages do not represent NO accumulation from LSM conditions.

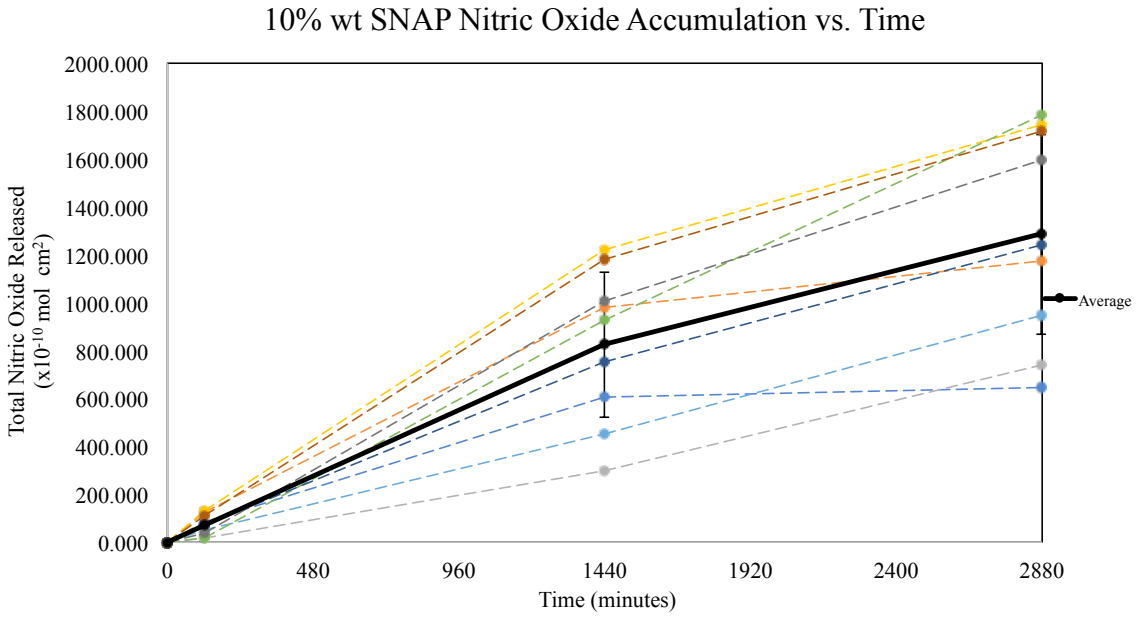

Figure 27: Mean NO accumulation averages for the 0, 2, 24, and 48 hour time points of nine 10 wt% SNAP films. Accumulation average (solid black line) is not a representative of individual 10 wt% SNAP NO accumulation.

Max/min accumulation for the 0, 2, 24, 48-hour times points (max/min) were measured at 0/0 $\frac{mol^{-10}}{cm^2}$, 17.215/131.647 $\frac{mol^{-10}}{cm^2}$, 295.126/1221.364 $\frac{mol^{-10}}{cm^2}$, and 646.549/1781.507 $\frac{mol^{-10}}{cm^2}$, respectively; the polymer exposed to liquid (1.001 cm^2) during incubation was estimated using

the surface area of a cone ($S.A = \pi r\left(r + \sqrt{r^2 + h^2}\right)$; h = 0.7 cm, r = 0.3 cm). NO accumulation measurements (Table 6**)** demonstrate the irregular accumulation of NO from 10 wt% SNAP films over 48 hours of incubation at 37°C. Overall, these results support that 10 wt% SNAP NO flux was variable and limited our ability to analyze the effects of 10 wt% polymer and NO release on LSM measurement; additionally, these variable effects might have interactions with glucose which was shown to influence fibrin clot measurements in the above section.

Table 6: Output of NO flux accumulation data from 10 wt% SNAP films over 48 hours at 37℃.

	NO Accumulation mol*cm^{-2}										
Time (minutes)	**Sample 1**	**Sample 2**	**Sample 3**	**Sample 4**	**Sample 5**	**Sample 6**	**Sample 7**	**Sample 8**	**Sample 9**	**Average**	**STD.P of Averages**
0	0.000	0.000	0.000	0.000	0.000	0.000	0.000	0.000	0.000	0.000	0.0000
120	82.132	121.268	17.215	131.647	49.835	18.105	69.754	113.900	34.152	70.890	41.7228
1440	602.588	980.748	295.126	1221.364	451.250	926.486	755.070	1179.571	1006.305	824.279	302.7761
2880	646.549	1172.448	739.104	1739.203	944.680	1781.507	1239.510	1716.537	1592.440	1285.775	417.6302

Fluorescence Data. Fluorescence data was collected to confirm the presence of tagged fibrinogen with polymer integration; 10.0mM2hrSNAP, 0.0mM48hrSNAP, 6.0mM48hrSNAP, and 10.0mM48hrSNAP conditions were suspected to measure lower in dyed fibrinogen concentration and explain consistent lack of detected fibrin fibers in these four conditions. The standard curve (Figure 28; $R^2 = 0.96$), linearly fit by plotting fluorescence vs. known dyed fibrinogen concentration, was considered when evaluating the effect of 10 wt% NAP/SNAP polymer exposure on dyed fibrinogen concentration. Fluorescence was converted into a more tangible measurement, dyed fibrinogen concentration (g/L) and compared to glucose conditions without polymer exposure; individual influences of glucose concentration and incubation material (i.e., polymer) on dyed fibrinogen concentration were examined separately using one-way ANOVA before analysis of interaction effects was considered.

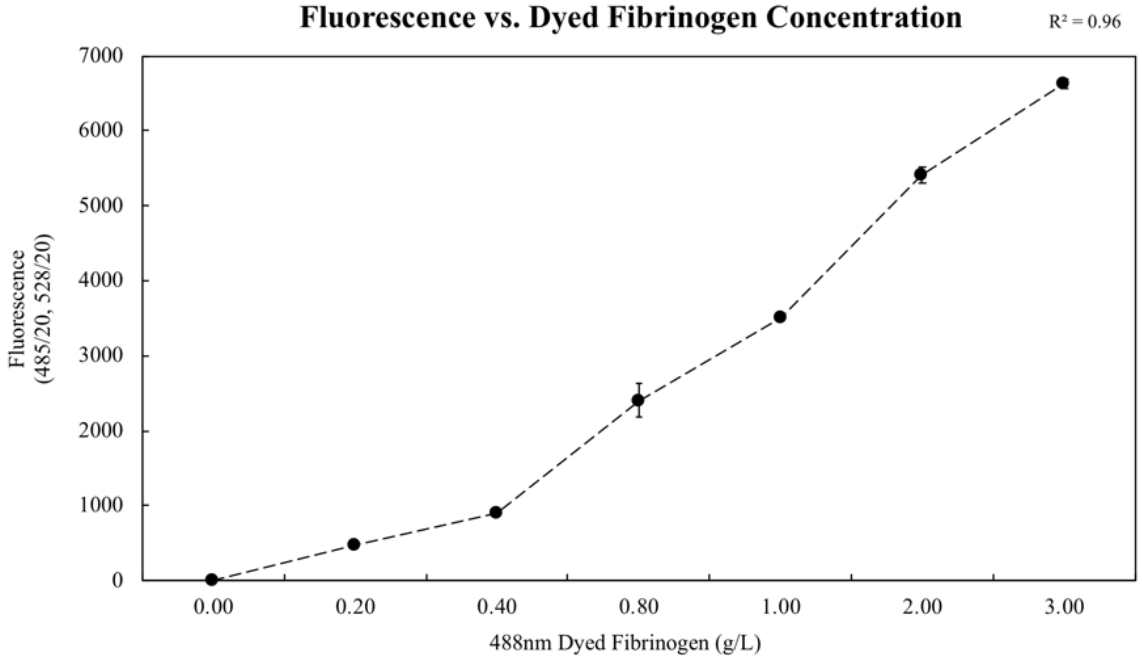

Figure 28: The standard curve ($R^2 = 0.96$) used to measure the concentration of dyed fibrinogen in 48 hour (glucose, 48hrNAP, and 48hrSNAP) incubated samples.

Dyed Fibrinogen Concentration vs. Glucose. Average dyed fibrinogen concentrations (Figure 29) for 0.0mM, 6.0mM, and 10.0mM glucose (e.g., 0.0mM + 0.0mM48hrNAP + 0.0mM48hrSNAP) were found to be 0.737 g/L, 0.684 g/L, and 0.562 g/L, respectively. One-way ANOVA found that glucose concentration significantly ($p > 0.1$) affected dyed fibrinogen concentration, and likewise, a mean statistical difference was found between 0.0mM and 10.0mM glucose conditions ($p < 0.05$).

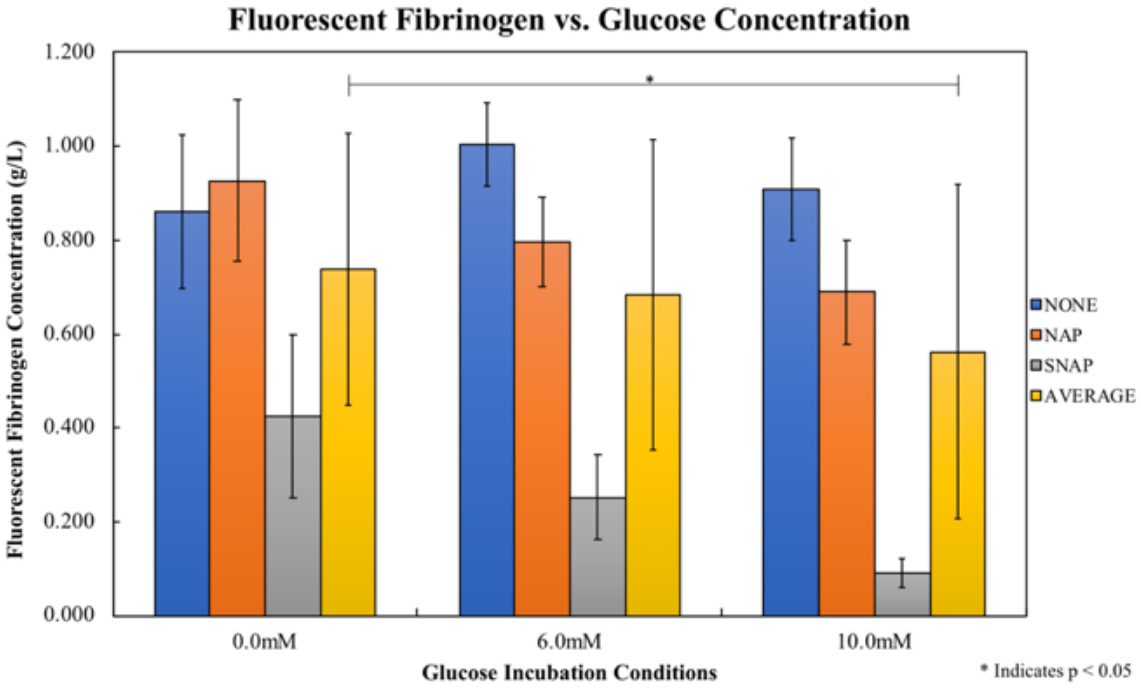

Figure 29: Dyed fibrinogen concentration vs. glucose concentration with averages and standard deviation bars. Statistical significance: * $p < 0.05$.

Dyed Fibrinogen Concentration vs. Incubation Material. In comparison, dyed fibrinogen concentration averages (Figure 30) for glucose, 48hrNAP, and 48hrSNAP (e.g., 0.0mM + 6.0mM +10.0mM) were found to be 0.924 g/L, 0.804 g/L, and 0.255 g/L, respectively. This influenced fibrin fiber characteristic measurements in LSM conditions by changing the availability of fibrinogen during polymerization with thrombin. One-way ANOVA found material incubation to significantly influence dyed fibrinogen concentration for both 10 wt% NAP ($p < 0.001$) and 10 wt% SNAP ($p < 0.0001$). Two-way ANOVA was not conducted on these data because glucose concentration was found to not significantly influence dyed fibrinogen concentration. Incubation material influence dyed fibrinogen concentration and generally supports LSM measurements from the four LSM conditions (10.0mM2hrSNAP, 0.0mM48hrSNAP, 6.0mM48hrSNAP, and 10.0mM48hrSNAP) in which polymerization did not

occur. Overall, fluorescence data found 48-hour 10 wt% SNAP exposure to reduce average dyed fibrinogen concentration by 72.36%.

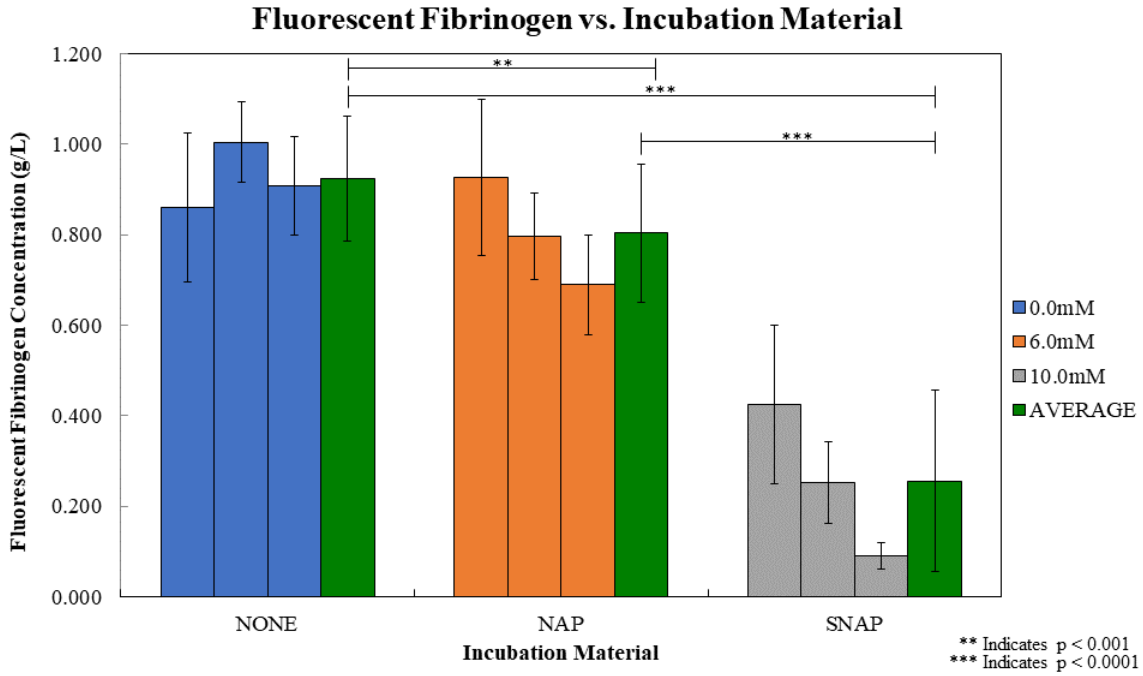

Figure 30: Dyed fibrinogen concentration vs. incubation material with averages and standard deviation bars. Statistical significance: ** $p < 0.001$, *** $p < 0.0001$.

5.3 Discussion

Methodologies were developed to examine NO-specific effects on fibrin clot characteristics through comparison to a non-NO releasing counterpart, but variable NO flux from 10 wt% SNAP polymer limited analysis of NO-specific effects on LSM measurements. Therefore, the main aim of this experimentation, to preliminarily examine the efficacy in utilizing 10 wt% SNAP to limit clot formation in hyperglycemic environments remained unanswered. However, four LSM conditions in which polymerization did not occur were from conditions incubated with 10 wt% SNAP. One theory to explain this phenomenon is the effect of some amount of NO accumulation on fibrinogen adhesion. Assuming fibrinogen adhesion to the polymer surface, fibrinogen would be bound to the polymer surface and not have been

transferred to the polymerization tube during LSM experimentation. While lower dyed fibrinogen concentration was also found in 48 hour 10 wt% NAP conditions (in comparison to original glucose conditions), 10 wt% SNAP measured significantly lower than both glucose and 10 wt% NAP dyed fibrinogen averages. Despite believed variability in NO release from 10wt% SNAP, these two findings suggest: 1) exposure of fibrinogen to NAP/SNAP polymer increases fibrinogen adsorption to its surface; and 2) the integration of SNAP, a NO-containing species, into the polymer further increases fibrinogen adsorption to the polymer surface.

Not only does an increased fibrinogen adhesion theory explain the lower dyed fibrinogen concentration from 48hrSNAP conditions, but more interestingly, justifies why 10.0mM48hrSNAP was the only 2-hour 10 wt% polymer condition (1 of 6) in which polymerization did not occur. From adsorption data, 10.0mM48hrSNAP glucose resulting in the lowest average dyed fibrinogen concentration (0.090 g/L). While this further supports an increased fibrinogen adhesion theory, exposure of 10 wt% SNAP to 10.0mM glucose fibrinogen solution causes adhesion within two hours; 2 hour conditions were pre-glycated prior to 10 wt% NAP/SNAP exposure and glucose study found glucose concentration to influence fibrinogen glycation and significantly higher in the 10.0mM condition. In summary, pre-glycated fibrinogen may also have a higher affinity for 10 wt% SNAP and could have clinical applications for limiting glycated fibrinogen's role in hemostatic response; further experimentation should examine adhesion effects on glycated fibrinogen for clinical applications.

Fibrinogen adhesion to Carbosil 2080 was measured previously, in which monolayers of fibrinogen adsorption were found on CarboSil 2080A surfaces [194]; Dow Corning® RTV 3140 Silicone Rubber, SP60D60, a hydrophilic antifouling polymer topcoat, and, SG80A, a Tecoflex® solution processable grade thermoplastic polyurethane resin, were also examined for anti-

thrombotic and anti-microbial applications, but only protein adhesion on SP60D60 (2.24 ± 0.68 nm) confirmed to be non-existent ($p = 0.004$). All of these polymers were integrated with 10 wt% SNAP and measured for NO flux, but CarboSil 2080a demonstrated superior NO release beyond 24 hours; higher release of NO from CarboSil 2080A, despite lower leaching, is an advantage of CarboSil 2080A because the material properties allow it to release NO without leaching SNAP. SP60D60 did not display prolonged NO release with 10 wt% SNAP integration, but was further used as a top coat with 10% SNAP CarboSil 2080A due to its effectiveness in reducing fibrinogen adhesion in previous examination. While fibrinogen adhesion was not tested on this composite polymer, the hydrophobic CarboSil 2080A was believed to provide sustained release of NO while the formation of hydration top layer on SP60D60 was expected to prevent protein attachment. The composite was examined for microbial growth and successfully reduced bacterial growth on the material's surface. Prevention of protein adhesion with SP60D60 could help reduce fibrinogen adhesion when examining NO specific effect on fibrin clot characteristics under LSM using our current methodology. However, other hydrophilic polymers may provide similar effects and should be further investigated when selecting the best polymer for further experimentation.

5.4 Conclusions

While the aim of this experimentation was to examine the efficacy in utilizing NO mechanisms to limit clot formation in hyperglycemic environments, experimentation did not result in any conclusion on 10%wt SNAP polymer's NO-specific effects because NO flux over 48 hours was variable. However, polymerization did not occur in the four LSM conditions. All four conditions were incubated with 10wt% SNAP and it is believed that some amount of NO accumulation increased fibrinogen adhesion to the polymer surface to cause fibrin fibers not to

form. This was supported by fluorescence data in which 48-hour incubation with 10 wt% SNAP reduced dyed fibrinogen concentration by an average of 72.36%. This effect was even more pronounced at 10.0mM glucose to explain why the only 2-hour exposure condition (1 of 6) in which polymerization did not occur was the 10.0mM48hr condition. Overall, fluorescence data suggests exposure of fibrinogen to NAP/SNAP polymer increased fibrinogen adsorption to its surface and integration of SNAP, a NO-containing species, into the polymer further increased fibrinogen adsorption to the polymer surface. Further experimentation should examine polymer adhesion effects on glycated fibrinogen for clinical applications.

BIBLIOGRAPHY

1. Stalker, T.J., J.D. Welsh, and L.F. Brass, *Shaping the platelet response to vascular injury.* Curr Opin Hematol, 2014. **21**(5): p. 410-7.
2. Singh, P., R. Kaur, and A. Kaur, *Clot composition and treatment approach to acute ischemic stroke: The road so far.* Ann Indian Acad Neurol, 2013. **16**(4): p. 494-7.
3. Komorowicz, E., et al., *Flow rate-modulated dissolution of fibrin with clot-embedded and circulating proteases.* Circ Res, 1998. **82**(10): p. 1102-8.
4. Mackman, N., *Triggers, targets and treatments for thrombosis.* Nature, 2008. **451**(7181): p. 914-8.
5. Doolittle, R.F., *Searching for differences between fibrinogen and fibrin that affect the initiation of fibrinolysis.* Cardiovasc Hematol Agents Med Chem, 2008. **6**(3): p. 181-9.
6. Shin, H.J., et al., *The effect of hyperglycemia on blood coagulation: In vitro, observational healthy-volunteer study using rotational thromboelastometry (ROTEM).* Medicine, 2016. **95**(35).
7. Norton, D.G., et al., *Computational imaging analysis of glycated fibrin gels reveals aggregated and anisotropic structures.* J Biomed Mater Res A, 2017. **105**(8): p. 2191-2198.
8. Fan, N.K., et al., *Experimental and imaging techniques for examining fibrin clot structures in normal and diseased states.* J Vis Exp, 2015(98): p. e52019.
9. Costa-Filho, R., et al., *Over 50 Years of Fibrinogen Concentrate.* Clin Appl Thromb Hemost, 2016. **22**(2): p. 109-14.
10. Silvain, J., et al., *Composition of coronary thrombus in acute myocardial infarction.* J Am Coll Cardiol, 2011. **57**(12): p. 1359-67.
11. Saito, H., T. Matsushita, and T. Kojima, *Historical perspective and future direction of coagulation research.* J Thromb Haemost, 2011. **9 Suppl 1**: p. 352-63.
12. Huang, S., et al., *Biosynthesis of human fibrinogen. Subunit interactions and potential intermediates in the assembly.* J Biol Chem, 1993. **268**(12): p. 8919-26.
13. Mosesson, M.W., *Fibrinogen and fibrin structure and functions.* J Thromb Haemost, 2005. **3**(8): p. 1894-904.
14. Huang, S., Z. Cao, and E.W. Davie, *The role of amino-terminal disulfide bonds in the structure and assembly of human fibrinogen.* Biochem Biophys Res Commun, 1993. **190**(2): p. 488-95.
15. Doolittle, R.F., *Fibrinogen and fibrin.* Annu Rev Biochem, 1984. **53**: p. 195-229.
16. McDowall, J. *Fibrinogen*. 2006; Available from: https://www.ebi.ac.uk/interpro/potm/2006_11/Page1.htm.
17. Weisel, J.W. and L. Medved, *The structure and function of the alpha C domains of fibrinogen.* Ann N Y Acad Sci, 2001. **936**: p. 312-27.
18. Chernysh, I.N., C. Nagaswami, and J.W. Weisel, *Visualization and identification of the structures formed during early stages of fibrin polymerization.* Blood, 2011. **117**(17): p. 4609-14.

19. Ferri, F., et al., *Structure of fibrin gels studied by elastic light scattering techniques: dependence of fractal dimension, gel crossover length, fiber diameter, and fiber density on monomer concentration.* Phys Rev E Stat Nonlin Soft Matter Phys, 2002. **66**(1 Pt 1): p. 011913.
20. Magatti, D., et al., *Modeling of fibrin gels based on confocal microscopy and light-scattering data.* Biophys J, 2013. **104**(5): p. 1151-9.
21. Litvinov, R.I., et al., *Polymerization of fibrin: Direct observation and quantification of individual B:b knob-hole interactions.* Blood, 2007. **109**(1): p. 130-8.
22. Weisel, J.W. and R.I. Litvinov, *Mechanisms of fibrin polymerization and clinical implications.* Blood, 2013. **121**(10): p. 1712-9.
23. Binnie, C.G. and S.T. Lord, *The Fibrinogen Sequences That Interact with Thrombin.* Blood, 1993. **81**(12): p. 3186-3192.
24. Cilia La Corte, A.L., H. Philippou, and R.A. Ariens, *Role of fibrin structure in thrombosis and vascular disease.* Adv Protein Chem Struct Biol, 2011. **83**: p. 75-127.
25. Hantgan, R.R. and J. Hermans, *Assembly of fibrin. A light scattering study.* J Biol Chem, 1979. **254**(22): p. 11272-81.
26. Fogelson, A.L. and J.P. Keener, *Toward an understanding of fibrin branching structure.* Phys Rev E Stat Nonlin Soft Matter Phys, 2010. **81**(5 Pt 1): p. 051922.
27. Ryan, E.A., et al., *Structural origins of fibrin clot rheology.* Biophys J, 1999. **77**(5): p. 2813-26.
28. Utah, T.U.o. *Physiological Gels Research Group*. 2017; Available from: https://www.math.utah.edu/research/mathbio/groups/gels/gel_fibrin_page.html.
29. Chernysh, I.N. and J.W. Weisel, *Dynamic imaging of fibrin network formation correlated with other measures of polymerization.* Blood, 2008. **111**(10): p. 4854-4861.
30. White, J.G., W.B. Amos, and M. Fordham, *An evaluation of confocal versus conventional imaging of biological structures by fluorescence light microscopy.* J Cell Biol, 1987. **105**(1): p. 41-8.
31. Crivat, G. and J.W. Taraska, *Imaging proteins inside cells with fluorescent tags.* Trends Biotechnol, 2012. **30**(1): p. 8-16.
32. Prasad, V., D. Semwogerere, and E.R. Weeks, *Confocal microscopy of colloids.* Journal of Physics-Condensed Matter, 2007. **19**(11).
33. Combs, C.A., *Fluorescence microscopy: a concise guide to current imaging methods.* Curr Protoc Neurosci, 2010. **Chapter 2**: p. Unit2 1.
34. Shashkova, S. and M.C. Leake, *Single-molecule fluorescence microscopy review: shedding new light on old problems.* Biosci Rep, 2017. **37**(4).
35. Chalfie, M., *GFP: Lighting up life.* Proc Natl Acad Sci U S A, 2009. **106**(25): p. 10073-80.
36. Chalfie, M., *Green fluorescent protein.* Photochem Photobiol, 1995. **62**(4): p. 651-6.
37. Giepmans, B.N., et al., *The fluorescent toolbox for assessing protein location and function.* Science, 2006. **312**(5771): p. 217-24.
38. Webb, D.J. and C.M. Brown, *Epi-fluorescence microscopy.* Methods Mol Biol, 2013. **931**: p. 29-59.
39. Zhang, L., et al., *Practical implementation, characterization and applications of a multi-colour time-gated luminescence microscope.* Sci Rep, 2014. **4**: p. 6597.
40. Thorn, K., *A quick guide to light microscopy in cell biology.* Mol Biol Cell, 2016. **27**(2): p. 219-22.

41. Rottenfusser, R. *Education in Microscopy and Digital Imaging*. 2016; Available from: http://zeiss-campus.magnet.fsu.edu.
42. Braat, J.J.M., et al., *Image formation in a multilayer using the Extended Nijboer-Zernike theory.* JEOS, 2009.
43. Weisshart, K. *The Basic Principle of Airyscanning*. July 2014; Available from: http://confocal-club.ru/upload/article/EN_wp_LSM-880_Basic-Principle-Airyscan.pdf.
44. Schermelleh, L., R. Heintzmann, and H. Leonhardt, *A guide to super-resolution fluorescence microscopy.* J Cell Biol, 2010. **190**(2): p. 165-75.
45. Hategan, A., et al., *Visualization of the dynamics of fibrin clot growth 1 molecule at a time by total internal reflection fluorescence microscopy.* Blood, 2013. **121**(8): p. 1455-8.
46. Collet, J.P., et al., *Influence of fibrin network conformation and fibrin fiber diameter on fibrinolysis speed: dynamic and structural approaches by confocal microscopy.* Arterioscler Thromb Vasc Biol, 2000. **20**(5): p. 1354-61.
47. Lang, N.R., et al., *Estimating the 3D pore size distribution of biopolymer networks from directionally biased data.* Biophys J, 2013. **105**(9): p. 1967-75.
48. Ferri, F., et al., *Growth kinetics and structure of fibrin gels.* Phys Rev E Stat Nonlin Soft Matter Phys, 2001. **63**(3 Pt 1): p. 031401.
49. Shah, G.A., et al., *Polydispersion in the diameter of fibers in fibrin networks: consequences on the measurement of mass-length ratio by permeability and turbidity.* Biopolymers, 1982. **21**(6): p. 1037-47.
50. Brown, A.C. and T.H. Barker, *Fibrin-based biomaterials: modulation of macroscopic properties through rational design at the molecular level.* Acta Biomater, 2014. **10**(4): p. 1502-14.
51. Brown, A.E., et al., *Multiscale mechanics of fibrin polymer: gel stretching with protein unfolding and loss of water.* Science, 2009. **325**(5941): p. 741-4.
52. Dickson, B.C., *Virchow's triad.* British Journal of Haematology, 2009. **145**(3): p. 433-433.
53. Makin, A., S.H. Silverman, and G.Y. Lip, *Peripheral vascular disease and Virchow's triad for thrombogenesis.* QJM, 2002. **95**(4): p. 199-210.
54. Nieuwdorp, M., et al., *Hypercoagulability in the metabolic syndrome.* Current Opinion in Pharmacology, 2005. **5**(2): p. 155-159.
55. Kumar, D.R., et al., *Virchow's contribution to the understanding of thrombosis and cellular biology.* Clin Med Res, 2010. **8**(3-4): p. 168-72.
56. Esmon, C.T., *Basic mechanisms and pathogenesis of venous thrombosis.* Blood Rev, 2009. **23**(5): p. 225-9.
57. Kyrle, P.A. and S. Eichinger, *Risk assessment for recurrent venous thrombosis reply.* Lancet, 2011. **377**(9771): p. 1073-1074.
58. Schafer, A.I., *The hypercoagulable states.* Ann Intern Med, 1985. **102**(6): p. 814-28.
59. Kitchens, C.S., *Concept of hypercoagulability: a review of its development, clinical application, and recent progress.* Semin Thromb Hemost, 1985. **11**(3): p. 293-315.
60. Kyrle, P.A. and S. Eichinger, *Deep vein thrombosis.* Lancet, 2005. **365**(9465): p. 1163-74.
61. van Es, N., et al., *Screening for cancer in patients with unprovoked venous thromboembolism: protocol for a systematic review and individual patient data meta-analysis.* BMJ Open, 2017. **7**(6): p. e015562.

62. Carr, M.E., *Diabetes mellitus: a hypercoagulable state.* J Diabetes Complications, 2001. **15**(1): p. 44-54.
63. Osende, J.I., et al., *Blood thrombogenicity in type 2 diabetes mellitus patients is associated with glycemic control.* J Am Coll Cardiol, 2001. **38**(5): p. 1307-12.
64. Lemkes, B.A., et al., *Hyperglycemia: a prothrombotic factor?* J Thromb Haemost, 2010. **8**(8): p. 1663-9.
65. Grant, P.J., *Diabetes mellitus as a prothrombotic condition.* Journal of Internal Medicine, 2007. **262**(2): p. 157-172.
66. Hull, C.M. and J.A. Harris, *Cardiology Patient Page. Venous thromboembolism and marathon athletes.* Circulation, 2013. **128**(25): p. e469-71.
67. American Diabetes, A., *Diagnosis and classification of diabetes mellitus.* Diabetes Care, 2009. **32 Suppl 1**: p. S62-7.
68. Haffner, S.M., *The metabolic syndrome: inflammation, diabetes mellitus, and cardiovascular disease.* Am J Cardiol, 2006. **97**(2A): p. 3A-11A.
69. Karamanou, M., et al., *Milestones in the history of diabetes mellitus: The main contributors.* World J Diabetes, 2016. **7**(1): p. 1-7.
70. Ahmed, A.M., *History of diabetes mellitus.* Saudi Med J, 2002. **23**(4): p. 373-8.
71. Olokoba, A.B., O.A. Obateru, and L.B. Olokoba, *Type 2 diabetes mellitus: a review of current trends.* Oman Med J, 2012. **27**(4): p. 269-73.
72. Mark Kirchhof, B.H., Meds 2009, B.H. Nooreen Popat, Meds 2008 , and B.H. Janet Malowany, Meds 2008, *Diagnostic Review: A Historical Perspective of the Diagnosis of Diabetes.* UWOMJ, 2008.
73. Tuomi, T., *Type 1 and type 2 diabetes: what do they have in common?* Diabetes, 2005. **54 Suppl 2**: p. S40-5.
74. Cheng, D., *Prevalence, predisposition and prevention of type II diabetes.* Nutr Metab (Lond), 2005. **2**: p. 29.
75. CDC. *Long-term Trends in Diabetes*. April 2017; Available from: https://www.cdc.gov/diabetes/statistics/slides/long_term_trends.pdf.
76. Mathers, C.D. and D. Loncar, *Projections of global mortality and burden of disease from 2002 to 2030.* PLoS Med, 2006. **3**(11): p. e442.
77. Forouhi, N.G. and N.J. Wareham, *Epidemiology of diabetes.* Medicine (Abingdon), 2014. **42**(12): p. 698-702.
78. Herman, W.H. and P. Zimmet, *Type 2 diabetes: an epidemic requiring global attention and urgent action.* Diabetes Care, 2012. **35**(5): p. 943-4.
79. Misra, A., N. Singhal, and L. Khurana, *Obesity, the metabolic syndrome, and type 2 diabetes in developing countries: role of dietary fats and oils.* J Am Coll Nutr, 2010. **29**(3 Suppl): p. 289S-301S.
80. American Diabetes, A., *Diagnosis and classification of diabetes mellitus.* Diabetes Care, 2014. **37 Suppl 1**: p. S81-90.
81. American Diabetes, A., *Economic costs of diabetes in the U.S. in 2012.* Diabetes Care, 2013. **36**(4): p. 1033-46.
82. Tabish, S.A., *Is Diabetes Becoming the Biggest Epidemic of the Twenty-first Century?* International Journal of Health Sciences, Qassim Universit, 2007. **Vol. 1**(No.2).
83. Zhuo, X., et al., *The lifetime cost of diabetes and its implications for diabetes prevention.* Diabetes Care, 2014. **37**(9): p. 2557-64.

84. Leung, M.Y., et al., *Life years lost and lifetime health care expenditures associated with diabetes in the U.S., National Health Interview Survey, 1997-2000.* Diabetes Care, 2015. **38**(3): p. 460-8.
85. Scott, R.A., et al., *A genomic approach to therapeutic target validation identifies a glucose-lowering GLP1R variant protective for coronary heart disease.* Science Translational Medicine, 2016. **8**(341).
86. Stewart, J., G. Manmathan, and P. Wilkinson, *Primary prevention of cardiovascular disease: A review of contemporary guidance and literature.* Jrsm Cardiovascular Disease, 2017. **6**.
87. Dobesh, P.P., *Economic burden of venous thromboembolism in hospitalized patients.* Pharmacotherapy, 2009. **29**(8): p. 943-53.
88. Engelgau, M.M., et al., *The evolving diabetes burden in the United States.* Ann Intern Med, 2004. **140**(11): p. 945-50.
89. Grundy, S.M., et al., *Diabetes and cardiovascular disease: a statement for healthcare professionals from the American Heart Association.* Circulation, 1999. **100**(10): p. 1134-46.
90. Heit, J.A., *Venous thromboembolism: disease burden, outcomes and risk factors.* J Thromb Haemost, 2005. **3**(8): p. 1611-7.
91. Petrauskiene, V., et al., *The risk of venous thromboembolism is markedly elevated in patients with diabetes.* Diabetologia, 2005. **48**(5): p. 1017-21.
92. Ageno, W., et al., *Cardiovascular risk factors and venous thromboembolism: a meta-analysis.* Circulation, 2008. **117**(1): p. 93-102.
93. Alzahrani, S.H. and R.A. Ajjan, *Coagulation and fibrinolysis in diabetes.* Diab Vasc Dis Res, 2010. **7**(4): p. 260-73.
94. Fuster, V. and B. Kelly, *Summary of the institute of medicine report promoting cardiovascular health in the developing world.* Glob Heart, 2011. **6**(4): p. 133-42.
95. Kucher, N., et al., *Risk factors associated with symptomatic pulmonary embolism in a large cohort of deep vein thrombosis patients.* Thromb Haemost, 2005. **93**(3): p. 494-8.
96. Perrier, A., *Deep vein thrombosis and pulmonary embolism: a single disease entity with different risk factors?* Chest, 2000. **118**(5): p. 1234-6.
97. Mahan, C.E., et al., *Venous thromboembolism: annualised United States models for total, hospital-acquired and preventable costs utilising long-term attack rates.* Thromb Haemost, 2012. **108**(2): p. 291-302.
98. Ageno, W., et al., *Risk factors for venous thromboembolism in the elderly: results of the master registry.* Blood Coagul Fibrinolysis, 2008. **19**(7): p. 663-7.
99. Tsai, A.W., et al., *Cardiovascular risk factors and venous thromboembolism incidence: the longitudinal investigation of thromboembolism etiology.* Arch Intern Med, 2002. **162**(10): p. 1182-9.
100. Ceriello, A., *Coagulation activation in diabetes mellitus:*
the role of hyperglycaemia and therapeutic prospects. Diabetologia, 1993.
101. Pieters, M., et al., *Glycaemic control improves fibrin network characteristics in type 2 diabetes - a purified fibrinogen model.* Thromb Haemost, 2008. **99**(4): p. 691-700.
102. Anderson, F.A., Jr. and F.A. Spencer, *Risk factors for venous thromboembolism.* Circulation, 2003. **107**(23 Suppl 1): p. I9-16.

103. Ten Cate, H., et al., *The role of platelets in venous thrombosis: a patient with Glanzmann's thrombasthenia and a factor V Leiden mutation suffering from deep venous thrombosis.* J Thromb Haemost, 2003. **1**(2): p. 394-5.
104. Montoro-Garcia, S., et al., *The Role of Platelets in Venous Thromboembolism.* Semin Thromb Hemost, 2016. **42**(3): p. 242-51.
105. Barazzoni, R., et al., *Increased fibrinogen production in type 2 diabetic patients without detectable vascular complications: Correlation with plasma glucagon concentrations.* Journal of Clinical Endocrinology & Metabolism, 2000. **85**(9): p. 3121-3125.
106. Bruno, G., et al., *Association of fibrinogen with glycemic control and albumin excretion rate in patients with non-insulin-dependent diabetes mellitus.* Annals of Internal Medicine, 1996. **125**(8): p. 653-657.
107. Mayne, E.E., J.M. Bridges, and J.A. Weaver, *Platelet Adhesiveness, Plasma Fibrinogen and Factor-Viii Levels in Diabetes Mellitus.* Diabetologia, 1970. **6**(4): p. 436-&.
108. Le, D.S., et al., *The association of plasma fibrinogen concentration with diabetic microvascular complications in young adults with early-onset of type 2 diabetes.* Diabetes Res Clin Pract, 2008. **82**(3): p. 317-23.
109. Bembde, A.S., *A study of plasma fibrinogen level in type-2 diabetes mellitus and its relation to glycemic control.* Indian J Hematol Blood Transfus, 2012. **28**(2): p. 105-8.
110. Suzuki, M., et al., *Laboratory evaluation of blood plasma separation device in children.* Pediatr Int, 2010. **52**(6): p. 891-2.
111. Lutjens, A., et al., *Glycosylation of human fibrinogen in vivo.* Diabetologia, 1985. **28**(2): p. 87-9.
112. Gugliucci, A., T. Menini, and A.J.C. Stahl, *Glycation of fibrinogen in diabetic patients: a practical colorimetric assay.* Glycosylation and Disease, 1994.
113. Pieters, M., et al., *Glycation of fibrinogen in uncontrolled diabetic patients and the effects of glycaemic control on fibrinogen glycation.* Thromb Res, 2007. **120**(3): p. 439-46.
114. Dunn, E.J., R.A. Ariens, and P.J. Grant, *The influence of type 2 diabetes on fibrin structure and function.* Diabetologia, 2005. **48**(6): p. 1198-206.
115. Dunn, E.J., et al., *Molecular mechanisms involved in the resistance of fibrin to clot lysis by plasmin in subjects with type 2 diabetes mellitus.* Diabetologia, 2006. **49**(5): p. 1071-80.
116. Yasuda, T., et al., *Quantitative analysis of survival of transplanted smooth muscle cells with real-time polymerase chain reaction.* J Thorac Cardiovasc Surg, 2005. **129**(4): p. 904-11.
117. Weisel, J.W., *The mechanical properties of fibrin for basic scientists and clinicians.* Biophysical Chemistry, 2004. **112**(2-3): p. 267-276.
118. Brownlee, M., H. Vlassara, and A. Cerami, *Nonenzymatic glycosylation reduces the susceptibility of fibrin to degradation by plasmin.* Diabetes, 1983. **32**(7): p. 680-4.
119. Carr, M.E., Jr. and B.M. Alving, *Effect of fibrin structure on plasmin-mediated dissolution of plasma clots.* Blood Coagul Fibrinolysis, 1995. **6**(6): p. 567-73.
120. Chapin, J.C. and K.A. Hajjar, *Fibrinolysis and the control of blood coagulation.* Blood Reviews, 2015. **29**(1): p. 17-24.
121. Le Feuvre, C., et al., *Cardiac events after low osmolar ionic or isosmolar nonionic contrast media utilization in the current era of coronary angioplasty.* Catheter Cardiovasc Interv, 2006. **67**(6): p. 852-8.

122. Marin, J. and M.A. Rodriguez-Martinez, *Role of vascular nitric oxide in physiological and pathological conditions.* Pharmacol Ther, 1997. **75**(2): p. 111-34.
123. Vural, K.M. and M. Bayazit, *Nitric oxide: implications for vascular and endovascular surgery.* Eur J Vasc Endovasc Surg, 2001. **22**(4): p. 285-93.
124. Radomski, M.W. and S. Moncada, *Regulation of vascular homeostasis by nitric oxide.* Thromb Haemost, 1993. **70**(1): p. 36-41.
125. Luo, J.D. and A.F. Chen, *Nitric oxide: a newly discovered function on wound healing.* Acta Pharmacol Sin, 2005. **26**(3): p. 259-64.
126. Kuo, P.C. and R.A. Schroeder, *The emerging multifaceted roles of nitric oxide.* Ann Surg, 1995. **221**(3): p. 220-35.
127. Radomski, M.W., R.M. Palmer, and S. Moncada, *The role of nitric oxide and cGMP in platelet adhesion to vascular endothelium.* Biochem Biophys Res Commun, 1987. **148**(3): p. 1482-9.
128. Lopez-Jaramillo, P., et al., *The role of the L-arginine-nitric oxide pathway in preeclampsia.* Ther Adv Cardiovasc Dis, 2008. **2**(4): p. 261-75.
129. Liu, X., et al., *Estimation of nitric oxide concentration in blood for different rates of generation. Evidence that intravascular nitric oxide levels are too low to exert physiological effects.* J Biol Chem, 2007. **282**(12): p. 8831-6.
130. Rosselli, M., P.J. Keller, and R.K. Dubey, *Role of nitric oxide in the biology, physiology and pathophysiology of reproduction.* Hum Reprod Update, 1998. **4**(1): p. 3-24.
131. Cockcroft, J.R., *Exploring vascular benefits of endothelium-derived nitric oxide.* Am J Hypertens, 2005. **18**(12 Pt 2): p. 177S-183S.
132. Jeffers, A., M.T. Gladwin, and D.B. Kim-Shapiro, *Computation of plasma hemoglobin nitric oxide scavenging in hemolytic anemias.* Free Radic Biol Med, 2006. **41**(10): p. 1557-65.
133. Henstridge, D.C., et al., *The effect of the nitric oxide donor sodium nitroprusside on glucose uptake in human primary skeletal muscle cells.* Nitric Oxide, 2009. **21**(2): p. 126-31.
134. Moncada, S. and A. Higgs, *The L-arginine-nitric oxide pathway.* N Engl J Med, 1993. **329**(27): p. 2002-12.
135. Miller, M.R. and I.L. Megson, *Recent developments in nitric oxide donor drugs.* Br J Pharmacol, 2007. **151**(3): p. 305-21.
136. Hogg, N., *Biological chemistry and clinical potential of S-nitrosothiols.* Free Radic Biol Med, 2000. **28**(10): p. 1478-86.
137. Zhang, Y. and N. Hogg, *S-Nitrosothiols: cellular formation and transport.* Free Radic Biol Med, 2005. **38**(7): p. 831-8.
138. Handa, H., et al., *Hemocompatibility Comparison of Biomedical Grade Polymers Using Rabbit Thrombogenicity Model for Preparing Nonthrombogenic Nitric Oxide Releasing Surfaces.* J Mater Chem B Mater Biol Med, 2014. **2**(8): p. 1059-1067.
139. Singh, R.J., et al., *Mechanism of nitric oxide release from S-nitrosothiols.* J Biol Chem, 1996. **271**(31): p. 18596-603.
140. Ren, H., et al., *Thromboresistant/anti-biofilm catheters via electrochemically modulated nitric oxide release.* Bioelectrochemistry, 2015. **104**: p. 10-6.
141. Goudie, M.J., et al., *Characterization of an S-nitroso-N-acetylpenicillamine-based nitric oxide releasing polymer from a translational perspective.* Int J Polym Mater, 2016. **65**(15): p. 769-778.

142. Qiao, S., et al., *D-Penicillamine targets metastatic melanoma cells with induction of the unfolded protein response (UPR) and Noxa (PMAIP1)-dependent mitochondrial apoptosis.* Apoptosis, 2012. **17**(10): p. 1079-94.
143. Vaughn, M.W., L. Kuo, and J.C. Liao, *Estimation of nitric oxide production and reaction rates in tissue by use of a mathematical model.* Am J Physiol, 1998. **274**(6 Pt 2): p. H2163-76.
144. Freedman, J.E. and J. Loscalzo, *Nitric oxide and its relationship to thrombotic disorders.* J Thromb Haemost, 2003. **1**(6): p. 1183-8.
145. Tayefeh, F., et al., *Thermoregulatory vasodilation increases the venous partial pressure of oxygen.* Anesth Analg, 1997. **85**(3): p. 657-62.
146. Megson, I.L., et al., *N-Substituted analogues of S-nitroso-N-acetyl-D,L-penicillamine: chemical stability and prolonged nitric oxide mediated vasodilatation in isolated rat femoral arteries.* Br J Pharmacol, 1999. **126**(3): p. 639-48.
147. Reutov, V.P. and E.G. Sorokina, *NO-synthase and nitrite-reductase components of nitric oxide cycle.* Biochemistry (Mosc), 1998. **63**(7): p. 874-84.
148. Brisbois, E.J., et al., *Reduction in Thrombosis and Bacterial Adhesion with 7 Day Implantation of S-Nitroso-N-acetylpenicillamine (SNAP)-Doped Elast-eon E2As Catheters in Sheep.* J Mater Chem B Mater Biol Med, 2015. **3**(8): p. 1639-1645.
149. Akhter, S., et al., *Evidence for S-nitrosothiol-dependent changes in fibrinogen that do not involve transnitrosation or thiolation.* Proc Natl Acad Sci U S A, 2002. **99**(14): p. 9172-7.
150. Gale, A.J., *Continuing education course #2: current understanding of hemostasis.* Toxicol Pathol, 2011. **39**(1): p. 273-80.
151. Jackson, S.P., W.S. Nesbitt, and E. Westein, *Dynamics of platelet thrombus formation.* J Thromb Haemost, 2009. **7 Suppl 1**: p. 17-20.
152. Broos, K., et al., *Platelets at work in primary hemostasis.* Blood Rev, 2011. **25**(4): p. 155-67.
153. Du, X., *Signaling and regulation of the platelet glycoprotein Ib-IX-V complex.* Curr Opin Hematol, 2007. **14**(3): p. 262-9.
154. Shultz, P.J. and L. Raij, *Endogenously synthesized nitric oxide prevents endotoxin-induced glomerular thrombosis.* J Clin Invest, 1992. **90**(5): p. 1718-25.
155. Freedman, J.E., et al., *Nitric oxide released from activated platelets inhibits platelet recruitment.* J Clin Invest, 1997. **100**(2): p. 350-6.
156. Martinez, A., et al., *Matrix metalloproteinase-2 in platelet adhesion to fibrinogen: interactions with nitric oxide.* Med Sci Monit, 2001. **7**(4): p. 646-51.
157. Brisbois, E.J., et al., *Long-term nitric oxide release and elevated temperature stability with S-nitroso-N-acetylpenicillamine (SNAP)-doped Elast-eon E2As polymer.* Biomaterials, 2013. **34**(28): p. 6957-66.
158. Bennett, J.S., *Platelet-fibrinogen interactions.* Ann N Y Acad Sci, 2001. **936**: p. 340-54.
159. Joo, S.J., *Mechanisms of Platelet Activation and Integrin alphaIIbeta3.* Korean Circ J, 2012. **42**(5): p. 295-301.
160. Balon, T.W. and J.L. Nadler, *Nitric oxide release is present from incubated skeletal muscle preparations.* J Appl Physiol (1985), 1994. **77**(6): p. 2519-21.
161. Higaki, Y., et al., *Nitric oxide increases glucose uptake through a mechanism that is distinct from the insulin and contraction pathways in rat skeletal muscle.* Diabetes, 2001. **50**(2): p. 241-7.

162. Bradley, S.J., B.A. Kingwell, and G.K. McConell, *Nitric oxide synthase inhibition reduces leg glucose uptake but not blood flow during dynamic exercise in humans.* Diabetes, 1999. **48**(9): p. 1815-21.
163. Kingwell, B.A., et al., *Nitric oxide synthase inhibition reduces glucose uptake during exercise in individuals with type 2 diabetes more than in control subjects.* Diabetes, 2002. **51**(8): p. 2572-80.
164. Young, M.E., G.K. Radda, and B. Leighton, *Nitric oxide stimulates glucose transport and metabolism in rat skeletal muscle in vitro.* Biochem J, 1997. **322 (Pt 1)**: p. 223-8.
165. McGrowder, D., D. Ragoobirsingh, and P. Brown, *Modulation of glucose uptake in adipose tissue by nitric oxide-generating compounds.* J Biosci, 2006. **31**(3): p. 347-54.
166. Bryan, S., et al., *The effect of nitric oxide inhibitors and Snitroso-Nacetylpenicillamine on glucose concentration in an animal model.* J Nat Sci Biol Med, 2011. **2**(1): p. 80-6.
167. McGrowder, D., D. Ragoobirsingh, and T. Dasgupta, *The enhancement of the hyperglycemic effect of S-nitrosoglutathione and S-nitroso-N-acetylpenicillamine by vitamin C in an animal model.* BMC Pharmacol, 2002. **2**: p. 18.
168. *Classification and diagnosis of diabetes mellitus and other categories of glucose intolerance. National Diabetes Data Group.* Diabetes, 1979. **28**(12): p. 1039-57.
169. Frangi, A., et al., *Multiscale vessel enhancement filtering.* MICCAI, 1998. **1496**: p. 130-137.
170. Aggarwal, N. and W.C. Karl, *Line detection in images through regularized Hough transform.* IEEE Trans Image Process, 2006. **15**(3): p. 582-91.
171. Spasovski, G., et al., *Clinical practice guideline on diagnosis and treatment of hyponatraemia.* Intensive Care Medicine, 2014. **40**(3): p. 320-331.
172. Inc., T.m., *Matlab, User's. Guide*. 1992: Natick, MA.
173. Evans, P.A., et al., *Gel point and fractal microstructure of incipient blood clots are significant new markers of hemostasis for healthy and anticoagulated blood.* Blood, 2010. **116**(17): p. 3341-3346.
174. Curtis, D.J., et al., *A study of microstructural templating in fibrin-thrombin gel networks by spectral and viscoelastic analysis.* Soft Matter, 2013. **9**(19): p. 4883-4889.
175. Weisel, J.W., *"Ta panta rhei".* Blood, 2010. **116**(17): p. 3123-3124.
176. Inc., S.I., *"SAS 9.4 for windows."*. 2012: Cary, NC, USA.
177. Pieters, M., et al., *Glycation of fibrinogen in uncontrolled diabetic patients and the effects of glycaemic control on fibrinogen glycation.* Thrombosis Research, 2007. **120**(3): p. 439-446.
178. da Costa, G., et al., *Beyond Genetic Factors in Familial Amyloidotic Polyneuropathy: Protein Glycation and the Loss of Fibrinogen's Chaperone Activity.* Plos One, 2011. **6**(10).
179. Collet, J.P., et al., *The elasticity of an individual fibrin fiber in a clot.* Proc Natl Acad Sci U S A, 2005. **102**(26): p. 9133-7.
180. Baradet, T.C., J.C. Haselgrove, and J.W. Weisel, *Three-dimensional reconstruction of fibrin clot networks from stereoscopic intermediate voltage electron microscope images and analysis of branching.* Biophys J, 1995. **68**(4): p. 1551-60.
181. Undas, A. and R.A. Ariens, *Fibrin clot structure and function: a role in the pathophysiology of arterial and venous thromboembolic diseases.* Arterioscler Thromb Vasc Biol, 2011. **31**(12): p. e88-99.

182. Li, W., et al., *Fibrin Fiber Stiffness Is Strongly Affected by Fiber Diameter, but Not by Fibrinogen Glycation.* Biophys J, 2016. **110**(6): p. 1400-10.
183. Fonseca, D., et al., *The role of fibrinogen glycation in ATTR: evidence for chaperone activity loss in disease.* Biochem J, 2016. **473**(14): p. 2225-37.
184. Stec, J.J., et al., *Association of fibrinogen with cardiovascular risk factors and cardiovascular disease in the Framingham Offspring Population.* Circulation, 2000. **102**(14): p. 1634-8.
185. Machlus, K.R., et al., *Causal relationship between hyperfibrinogenemia, thrombosis, and resistance to thrombolysis in mice.* Blood, 2011. **117**(18): p. 4953-63.
186. Barazzoni, R., et al., *Increased fibrinogen production in type 2 diabetic patients without detectable vascular complications: correlation with plasma glucagon concentrations.* J Clin Endocrinol Metab, 2000. **85**(9): p. 3121-5.
187. Curtis, D.J., et al., *Rheometrical and molecular dynamics simulation studies of incipient clot formation in fibrin-thrombin gels: An activation limited aggregation approach.* Journal of Non-Newtonian Fluid Mechanics, 2011. **166**(16): p. 932-938.
188. Lawrence, M.J., et al., *Fractal dimension: A novel clot microstructure biomarker use in ST elevation myocardial infarction patients.* Atherosclerosis, 2015. **240**(2): p. 402-407.
189. D'silva, L., et al., *Defining the reference range for blood clot gel point and fractal dimension.* Journal of Thrombosis and Haemostasis, 2015. **13**: p. 538-538.
190. Evans, P.A., et al., *Gel point and fractal microstructure of incipient blood clots are significant new markers of hemostasis for healthy and anticoagulated blood.* Blood, 2010. **116**(17): p. 3341-6.
191. Undas, A., et al., *Hyperglycemia is associated with enhanced thrombin formation, platelet activation and fibrin clot resistance to lysis in patients with acute coronary syndrome.* European Heart Journal, 2008. **29**: p. 388-388.
192. Viswanathan, G.N., et al., *Differences in thrombus structure and kinetics in patients with type 2 diabetes mellitus after non ST elevation acute coronary syndrome.* Thrombosis Research, 2014. **133**(5): p. 880-885.
193. Chipinda, I. and R.H. Simoyi, *Formation and stability of a nitric oxide donor: S-nitroso-N-acetylpenicillamine.* J Phys Chem B, 2006. **110**(10): p. 5052-61.
194. Singha, P., et al., *Enhanced antibacterial efficacy of nitric oxide releasing thermoplastic polyurethanes with antifouling hydrophilic topcoats.* Biomater Sci, 2017. **5**(7): p. 1246-1255.

APPENDIX A

Image Processing Algorithm

Fibrin Overlap, Fiber Length, and Matrix Porosity MatLab Code:
Download and Install the Image Processing Toolbox

```
clc;clear; close all;

stack_prefix='0.0mM zstack1_';
doplot=false;

fibrin_fiber_overlap_agg = [];
long_aggr = [];
perc_porous = [];

for istack=1: AAAA
%istack is one more than the stack number in the filename
fn = strcat(strcat(stack_prefix,int2str(istack-1)),'.tif')
I = imread(fn);
BW1=im2bw(I,graythresh(I));
BW2=imadjust(mat2gray(BW1));
BW3 = fibermetric(BW2, 30, 'StructureSensitivity', 15);
BW = BW3 > 0.00002;

%BW tubular filter above misses the most intense areas (HOT)
HOT1=imadjust(I,[0.97 1.0],[]);
HOT2=im2bw(HOT1,graythresh(HOT1));
HOT3=imadjust(mat2gray(HOT2));
HOT4=imboxfilt(HOT3,25);
HOT = HOT4 > 0.6;

%add the most intense (HOT) back to the tubular(BW) results
BW = BW + HOT;

if doplot
   figure, imshowpair(I,BW,'montage'), hold on;
end

[H,T,R] = hough(BW);
P  = houghpeaks(H,400,'threshold',ceil(0.4*max(H(:))));
x = T(P(:,2)); y = R(P(:,1));
```

```
%plot(x,y,'s','Color','blue');

%lines = houghlines(BW,T,R,P,'FillGap',3,'MinLength',35);
lines = houghlines(BW,T,R,P,'FillGap',15,'MinLength',40);
linelen = [];
for k = 1:length(lines)
  xy = [lines(k).point1; lines(k).point2];

  if doplot
    plot(xy(:,1),xy(:,2),'LineWidth',2,'Color','red');
    % Plot beginnings and ends of lines
    %plot(xy(1,1),xy(1,2),'x','LineWidth',2,'Color','yellow');
    %plot(xy(2,1),xy(2,2),'x','LineWidth',2,'Color','blue');
  end

  linelen(k) = norm(lines(k).point1 - lines(k).point2);
end

% fibrin fiber overlap aggregation
% calc number intersections with other lines, average
numlineintersect = [];
for k = 1:length(lines)
  xy = [lines(k).point1; lines(k).point2];
  numlineintersect(k) = 0;
  for m = 1:length(lines)
    xy_m = [lines(m).point1; lines(m).point2];
    % https://www.mathworks.com/matlabcentral/fileexchange/27205-fast-line-segment-
intersection
    out = lineSegmentIntersect([xy(1,1) xy(1,2) xy(2,1) xy(2,2)],[xy_m(1,1) xy_m(1,2)
xy_m(2,1) xy_m(2,2)]);
    % https://www.mathworks.com/matlabcentral/fileexchange/56835-lineintersection
    %[E, lambda, gamma, isConvex] = lineIntersection(xy(:,1),xy(:,2),xy_m(:,1),xy_m(:,2));
    %if not(isnan(E))
    if (out.intMatrixX>0 && out.intMatrixY>0)
       numlineintersect(k) = numlineintersect(k)+1;
    end
  end
end

% fibrin fiber overlap aggregation, average lineintersect
fibrin_fiber_overlap_agg(istack) = mean(numlineintersect);

% elongation, logitudinal aggregation = average length of line segments
long_aggr(istack) = mean(linelen);

% percent porosity
```

```
[s1,s2]=size(BW);
tarea=(s1*s2);
perc_porous(istack) = (tarea-bwarea(BW))/tarea;

%imwrite(label2rgb(Pr_L),'Output.png')
end;

for istack=1:2 %83
sprintf('%d %12.4f %12.4f
%12.4f\n',istack,fibrin_fiber_overlap_agg(istack),long_aggr(istack),perc_porous(istack))
end;
```

Fractal Dimension Code:

```
clc;clear; close all;

stack_prefix= 'INC repeat zstack1_z';
doplot = false; %set AS true to print each image

for istack=1:10
%istack is one more than the stack number in the filename
   fn = strcat(strcat(stack_prefix,int2str(istack-1)),'.tif')
   I = imread(fn);

% Pad the image with background pixels so that its dimensions are a power of 2.
   maxDim = max(size(I));
   newDimSize = 2^ceil(log2(maxDim));
   rowPad = newDimSize - size(I, 1);
   colPad = newDimSize - size(I, 2);
   I = padarray(I, [rowPad, colPad], 'post');

   boxCounts = zeros(1, ceil(log2(maxDim)));
   resolutions = zeros(1, ceil(log2(maxDim)));

   boxSize = size(I, 1);
   boxesPerDim = 1;
   idx = 0;
   while boxSize >= 1
      boxCount = 0;

      for boxRow = 1:boxesPerDim
         for boxCol = 1:boxesPerDim
            minRow = (boxRow - 1) * boxSize + 1;
            maxRow = boxRow * boxSize;
            minCol = (boxCol - 1) * boxSize + 1;
            maxCol = boxCol * boxSize;
```

```
            objFound = false;
            for row = minRow:maxRow
               for col = minCol:maxCol
                  if I(row, col)
                     boxCount = boxCount + 1;
                     objFound = true; % Break from nested loop.
                  end;

                  if objFound
                     break; % Break from nested loop.
                  end;
               end;

               if objFound
                  break; % Break from nested loop.
               end;
            end;
         end;
      end;

      idx = idx + 1;
      boxCounts(idx) = boxCount;
      resolutions(idx) = 1 / boxSize;

      boxesPerDim = boxesPerDim * 2;
      boxSize = boxSize / 2;
   end;

   D = polyfit(log(resolutions), log(boxCounts), 1);
   D = D(1);
End
```

APPENDIX B

Fiber Overlap Code

```
data jacob.NEW_All_Glucose;
set jacob.All_Glucose;
if GLUCOSE = 0 then GLUCgrp = 1;
if GLUCOSE = 6 then GLUCgrp = 2;
if GLUCOSE = 10 then GLUCgrp = 3;
LABEL GLUCgrp = 'GLUCOSE Grouping';
RUN;
proc format;
value GLUCgrp 1 = 'INC' 2 = '6.0mM' 3 = '10.0mM'; run;

/*******************************************/
/*** THESIS - 1-WAY ANOVA NEW_ALL_GLUCOSE ***/
/*******************************************/
ods html close;
ods listing;
/* get simple summary statistics (sample size, sample mean and SD) with max of 2 decimal places) */
proc means  data=jacob.new_all_glucose maxdec=2 n mean std;
title2 'simple summary statistics FibOlap';
by GLUCgrp;  /* statistics computed for each glucose level */
var FibOlap;  /* FibOlap */
format GLUCgrp GLUCgrp.;
run;
proc plot data=jacob.new_all_glucose;
/* request a plot of raw FibOlap */
title2 'plot of the raw FibOlap data';
plot FibOlap*GLUCgrp;
format GLUCgrp GLUCgrp.;
run;
proc anova data=jacob.new_all_glucose;
title2 'Analysis FibOlap';
class GLUCgrp;
/* class statement indicates that GLUCgrp is a factor */
model FibOlap = GLUCgrp;
/* assumes GLUCgrp influences FibOlap */
means GLUCgrp / tukey cldiff;
/* multiple comparison by Tukey's method -- get actual C.I.'s */
means GLUCgrp / tukey lines;
format GLUCgrp GLUCgrp.;
run;
/* get pictorial display of comparisons */
proc glm data=jacob.new_all_glucose;
title2 'Proc glm Analysis FibOlap';
/* same as 'proc anova' except glm allows residual plots but gives more junk output */
class GLUCgrp;
model FibOlap = GLUCgrp;
output out=jacob.FibOlapfit p=yhat r=resid;
format GLUCgrp GLUCgrp.; run;
/* store fitted values and fitted residuals in dataset called FibOlapfit for later use */
proc univariate data=jacob.FibOlapfit plot normal;
var resid; run;
/* plot qq-plot of fitted residuals */
proc plot;
plot resid*type;
```

```
plot resid*yhat;
format GLUCgrp GLUCgrp.;
/* two residual plots to check independence and constant variance */
run;
```

Page Break

Fiber Length Code

```
/*** GLUCOSE - FibLen ***/
/* get simple summary statistics (sample size, sample mean and SD) with max
of 2 decimal places) */
proc means  data=jacob.new_all_glucose maxdec=2 n mean std;
title2 'simple summary statistics for FibLen';
by GLUCgrp;  /* statistics computed for each glucose level */
var FibLen;  /* FibLen */
format GLUCgrp GLUCgrp.;
run;
proc plot data=jacob.new_all_glucose;
/* request a plot of raw FibLen */
title2 'plot of the raw FibLen data';
plot FibLen*GLUCgrp;
format GLUCgrp GLUCgrp.;
run;
proc anova  data=jacob.new_all_glucose;
title2 'Analysis FibLen';
class GLUCgrp;
/* class statement indicates that GLUCgrp is a factor */
model FibLen = GLUCgrp;
/* assumes GLUCgrp influences FibLen */
means GLUCgrp / tukey cldiff;
/* multiple comparison by Tukey's method -- get actual C.I.'s */
means GLUCgrp / tukey lines;
format GLUCgrp GLUCgrp.;
run;
/* get pictorial display of comparisons */
proc glm data=jacob.new_all_glucose;
title2 'Proc glm Analysis FibLen';
/* same as 'proc anova' except glm allows residual plots but gives more junk
output */
class GLUCgrp;
model FibLen = GLUCgrp;
format GLUCgrp GLUCgrp.;
output out=jacob.FibLenfit p=yhat r=resid; run;
/* store fitted values and fitted residuals in dataset called FibLenfit for
later use */
proc univariate data=jacob.FibLenfit plot normal;
var resid; format GLUCgrp GLUCgrp.;run;
/* plot qq-plot of fitted residuals */
proc plot;
plot resid*type;
plot resid*yhat;
format GLUCgrp GLUCgrp.;
/* two residual plots to check independence and constant variance */
run;
```

.....Column Break.....**Matrix Porosity Code**

```
/*** GLUCOSE - FibMtrxPoro ***/
/* get simple summary statistics (sample size, sample mean and SD) with max
of 2 decimal places) */
```

```
proc means  data=jacob.new_all_glucose maxdec=2 n mean std;
title2 'simple summary statistics for FibMtrxPoro';
by GLUCgrp;  /* statistics computed for each glucose level */
var FibMtrxPoro;  /* FibMtrxPoro */
format GLUCgrp GLUCgrp.;
run;
proc plot data=jacob.new_all_glucose;
/* request a plot of raw FibMtrxPoro */
title2 'plot of the raw FibMtrxPoro data';
plot FibMtrxPoro*GLUCgrp;
format GLUCgrp GLUCgrp.;
run;
proc anova  data=jacob.new_all_glucose;
title2 'Analysis FibMtrxPoro';
class GLUCgrp;
/* class statement indicates that GLUCgrp is a factor */
model FibMtrxPoro = GLUCgrp;
/* assumes GLUCgrp influences FibMtrxPoro */
means GLUCgrp / tukey cldiff;
/* multiple comparison by Tukey's method -- get actual C.I.'s */
means GLUCgrp / tukey lines;
format GLUCgrp GLUCgrp.;
run;
/* get pictorial display of comparisons */
proc glm data=jacob.new_all_glucose;
title2 'Proc glm Analysis FibMtrxPoro';
/* same as 'proc anova' except glm allows residual plots but gives more junk
output */
class GLUCgrp;
model FibMtrxPoro = GLUCgrp;
format GLUCgrp GLUCgrp.;
output out=jacob.FibMtrxPorofit p=yhat r=resid; run;
/* store fitted values and fitted residuals in dataset called FibMtrxPorofit
for later use */
proc univariate data=jacob.FibMtrxPorofit plot normal;
var resid; format GLUCgrp GLUCgrp.;run;
/* plot qq-plot of fitted residuals */
proc plot;
plot resid*type;
plot resid*yhat;
format GLUCgrp GLUCgrp.;
/* two residual plots to check independence and constant variance */
run;
```